Master's thesis

NTNU
Norwegian University of Science and Technology
Faculty of Engineering
Department of Structural Engineering

Ine Amalie Seim Hermansen
Marie Elise McGeorge

Shear Capacity of Axially Loaded Concrete Beams without Transverse Reinforcement

Master's thesis in Civil and Environmental Engineering
Supervisor: Jan Arve Øverli
June 2020

NTNU
Norwegian University of Science and Technology

DNV·GL

Ine Amalie Seim Hermansen
Marie Elise McGeorge

Shear Capacity of Axially Loaded Concrete Beams without Transverse Reinforcement

Master's thesis in Civil and Environmental Engineering
Supervisor: Jan Arve Øverli
June 2020

Norwegian University of Science and Technology
Faculty of Engineering
Department of Structural Engineering

NTNU
Norwegian University of
Science and Technology

Department of Structural Engineering
Faculty of Engineering
NTNU – Norwegian University of Science and Technology

ACCESSIBILITY

Open

MASTER THESIS 2020

SUBJECT AREA: Concrete structures	DATE: 10/06/2020	NO. OF PAGES: 32+21 (Appendix)

TITLE:

Shear Capacity of Axially Loaded Concrete Beams without Shear Reinforcement

Skjærkapasitet i betongbjelker uten skjærarmering ved påført aksiallast

BY:

Ine Amalie Seim Hermansen and Marie Elise McGeorge

SUMMARY:
Concrete beams are common load-bearing members in structures such as buildings, bridges and offshore structures, where they are exposed to different types of load. Their capacity to resist these loads depends, not only on the magnitude of the loads, but also on how the loads are combined. Compression stress, caused by either applied axial forces or by prestressed reinforcement, is known to increase the shear capacity of a concrete specimen. However, as the standards used today are often based on empirical models when calculating shear in members without transverse reinforcement, there are some uncertainties as to how the shear capacity is affected when the axial load reaches larger magnitudes.

This paper investigates the shear capacity and mechanical behaviour of concrete beams without shear reinforcement, subjected to large axial loading. Nine shear-critical concrete beams were subjected to a four-point test until failure. The beams were divided into three sets prior to testing. The first set was considered as a reference set, and these beams were tested without any axial load. An axial load of 500 kN was applied to the beams in the second set, and an axial load of 800 kN was applied to the beams in the third set.

All the beams reached shear failure during the four-point test, where the beams without any axial load reached inclined tension failure and the beams with axial load reached shear compression failure. The testing showed that the shear capacity of the beams increased with the magnitude of the applied axial load, and a linear relationship was observed between the load and the capacity.

The results were compared to calculated shear capacities from the standards Eurocode NS-EN 1992-1-1:2004+A1:2014 +NA:2018 (Eurocode 2) and DNVGL-ST-C502, in order to see if the empirically based equations in these standards would be accurate for beams with large axial loads. When using the average concrete strength and omitting all safety and material factors from the equations, the calculated values from DNVGL-ST-C502 gave a better estimation for the test beams with high axial loading, and Eurocode 2 gave more accurate calculations for the beams without any axial load. While the Eurocode 2 seems to overestimate the effect of compressive stress on the shear capacity, axial loading seems to have a more limited impact on the calculated shear capacity from DNVGL-ST-C502.

RESPONSIBLE TEACHER: Jan Arve Øverli

SUPERVISOR(S): Jan Arve Øverli and Paola Mayorca

CARRIED OUT AT: Department of Structural Engineering and at DNV GL

Preface

This thesis was made for the Department of Structural Engineering at the Norwegian University of Science and Technology (NTNU), and it was produced in cooperation between NTNU and DNV GL. The report was written over the course of 20 weeks, from January to June 2020, and is the conclusion to our master's degree in structural engineering.

The main objective of this project was to see how a large axial compression load would affect the shear capacity of concrete beams without shear reinforcement. This was analysed by testing beams subjected to different magnitudes of axial load in a four-point test until failure, and the following article compares the obtained shear capacities in the beams.

As the analysis is based on experimental test results, the thesis was written as a scientific article. The article begins with a chapter on the theory behind shear failure and how axial compression can affect the shear capacity of concrete beams without shear reinforcement. This is followed by a chapter on how the topic is regarded in the standards Eurocode 2 and DNVGL-ST-C502. The rest of the article follows a characteristic set-up, where the experimental program is described and the test results are presented and discussed.

We would like to thank our supervisor at NTNU, Jan Arve Øverli, for all of his help, guidance and constructive criticism during this project. Special thanks are also directed to our supervisor at DNV GL, Paola Mayorca, and to Remi Fosse at DNV GL for answering all our emails regarding the shear topic in the standards.

This semester was heavily influenced by the outbreak of COVID-19 and the following lockdown of the Norwegian society. We would therefore like to especially thank Remi Fosse and the staff at the DNV GL laboratory in Høvik for performing the lab testing, sending us pictures and keeping us updated when we were prevented from being present in the lab ourselves. Additionally, we want to say thank you to Thomas Andersen, Geir Udahl and the workers at Contiga for their hospitality when the beams were produced, and for their extensive help in ensuring that the last test beams were properly stored after lockdown. We also want to express our gratitude to Erik Sveen and the staff at Statens Vegvesen in Lillehammer for testing the concrete cubes in their laboratory at very short notice, when it was no longer possible to conduct these tests at the DNV GL lab in Høvik.

Finally, we want to thank our families and friends for their help and support throughout our master studies.

Trondheim, 10th of June 2020

Ine Amalie Seim Hermansen

Marie Elise McGeorge

Abstract

Concrete beams are common load-bearing members in structures such as buildings, bridges and offshore structures, where they are exposed to different types of load. Their capacity to resist these loads depends, not only on the magnitude of the loads, but also on how the loads are combined. Compression stress, caused by either applied axial forces or by prestressed reinforcement, is known to increase the shear capacity of a concrete specimen. However, as the standards used today are often based on empirical models when calculating shear in members without transverse reinforcement, there are some uncertainties as to how the shear capacity is affected when the axial load reaches larger magnitudes.

This paper investigates the shear capacity and mechanical behaviour of concrete beams without shear reinforcement, subjected to large axial loading. Nine shear-critical concrete beams were subjected to a four-point test until failure. The beams were divided into three sets prior to testing. The first set was considered as a reference set, and these beams were tested without any axial load. An axial load of 500 kN was applied to the beams in the second set, and an axial load of 800 kN was applied to the beams in the third set.

All the beams reached shear failure during the four-point test, where the beams without any axial load reached inclined tension failure and the beams with axial load reached shear compression failure. The testing showed that the shear capacity of the beams increased with the magnitude of applied axial load, and a linear relationship was observed between the load and the capacity.

The results were compared to calculated shear capacities from the standards Eurocode NS-EN 1992-1-1:2004+A1:2014 +NA:2018 (Eurocode 2) and DNVGL-ST-C502, in order to see if the empirically based equations in these standards would be accurate for beams with large axial loads. When using the average concrete strength and omitting all safety and material factors from the equations, the calculated values from DNVGL-ST-C502 gave a better estimation for the test beams with high axial loading, and Eurocode 2 gave more accurate calculations for the beams without any axial load. While the Eurocode 2 seems to overestimate the effect of compressive stress on the shear capacity, axial loading seems to have a more limited impact on the calculated shear capacity from DNVGL-ST-C502.

Sammendrag

Betongbjelker blir ofte brukt som lastbærende elementer i blant annet bygninger, broer og i offshorekonstruksjoner, hvor de utsettes for forskjellige lastvirkninger. Kapasiteten til bjelkene avhenger både av størrelsen på hver lastvirkning, og på hvordan lastene kombineres. Aksielle trykkspenninger, forårsaket av forspent armering eller ytre laster, vil øke skjærkapasiteten til konstruksjonsdeler i betong. Ettersom dagens standarder i hovedsak baserer seg på empiriske modeller for skjærberegning i konstruksjonsdeler uten skjærarmering, er det likevel noe usikkerhet knyttet til hvordan skjærkapasiteten vil påvirkes ved stor aksialkraft.

Denne artikkelen ser på skjærkapasiteten og den mekaniske oppførselen til betongbjelker uten skjærarmering som er utsatt for aksiell trykklast. Ni skjærkritiske bjelker ble utsatt for en firepunkts-test til brudd. Bjelkene ble delt inn i tre sett før testene startet. Det første settet var et referansesett, og disse bjelkene ble testet uten aksiallast. Bjelkene fra det andre settet ble påført en aksialkraft på 500 kN, og bjelkene fra det tredje settet ble påført en aksialkraft på 800 kN. Alle bjelkene gikk til skjærbrudd under testingen. Bjelkene uten aksialkraft fikk diagonalt strekkbrudd, mens bjelkene med aksialkraft fikk skjær-trykkbrudd. Resultatene fra testingen viste at skjærkapasiteten økte med aksiallasten, og at forholdet mellom disse størrelse kunne beskrives som lineært.

For å kontrollere nøyaktigheten av empiriske formelverk ved stor aksiallast, ble resultatene sammenlignet med utregnede skjærkapasiteter fra standardene Eurokode NS-EN 1992-1-1:2004+A1:2014 +NA:2018 (Eurokode 2) og DNVGL-ST-C502. De utregnede verdiene baserte seg på middelfastheten i betongbjelkene, uten sikkerhets- og materialfaktorer. Resultatene fra DNVGL-ST-C502 traff da bedre for bjelkene med aksiallast, og Eurokode 2 ga et mer nøyatig resultat for bjelkene uten. Mens det virker som at Eurokodens formler for skjærkapasitet overvurderer effekten av aksiallast på skjærkapasiteten, hadde aksiallasten en mer begrenset innvirkning på den utregnede kapasiteten fra DNVGL-ST-C502.

Contents

Shear Capacity of Axially Loaded Concrete Beams without Transverse Reinforcement

Marie McGeorge, Ine Hermansen

Department of Structural Engineering, Faculty of Engineering, NTNU

Abstract

Concrete beams are common load-bearing members in structures such as buildings, bridges and offshore structures, where they are exposed to different kinds of loading. Their capacity to resist these loads depends, not only on the magnitude of the loads, but also on how they are combined. Compression stress, caused by either applied axial forces or by prestressed reinforcement, is known to increase the shear capacity of a concrete specimen. However, as the standards used today are often based on empirical models when calculating shear in members without transverse reinforcement, there are some uncertainties as to how the shear capacity is affected when the axial load reaches larger magnitudes.

This paper investigates the shear capacity and mechanical behaviour of concrete beams without shear reinforcement, subjected to large axial loading. Nine shear-critical concrete beams were divided into sets, where one set was without any axial load, and the other two sets were loaded with axial forces of 500 kN and 800 kN, respectively. The test beams were then subjected to a four-point loading test until failure. The observed capacities were compared to the calculated shear capacities from the standards Eurocode NS-EN 1992-1-1:2004+A1:2014 +NA:2018 (Eurocode 2) and DNVGL-ST-C502, in order to see if the empirically based equations in these standards would be accurate for large axial loads.

All the beams reached shear failure during the four-point test, where the beams without any axial load reached inclined tension failure and the beams with axial load reached shear compression failure. The testing showed that the shear capacity of the beams increased with the magnitude of applied axial load, and a linear relationship was observed between the load and the capacity.

The calculated values from DNVGL-ST-C502 were more accurate for the test beams with high axial loading, while the Eurocode gave more accurate calculations for the beams without any axial load. While the Eurocode 2 seems to overestimate the effect of compressive stress on the shear capacity, axial loading seems to have a more limited impact on the calculated capacity from DNVGL-ST-C502.

Keywords: Mechanical Behaviour, Shear Capacity, Axial Load, Beams

1 Introduction

The capacity of concrete beams will be affected by the magnitude of axial loading. Compression stress, caused by either applied axial forces or by prestressed reinforcement, will increase the shear capacity of the concrete and allow for larger shear loads before the specimen reaches failure. Conversely, an axial load in tension will have a negative effect on the shear capacity. This effect is taken into account in the standards and regulations that are used today [13]. However,

there are some uncertainties regarding this effect when the axial stress reaches a larger magnitude than what is usually found in concrete structures.

Shear is a disputed topic among researchers, especially when considering members without transverse reinforcement [2]. It has been the subject of many research projects to find a mechanical model with the ability to fully predict and explain the mechanisms behind shear failure in this type of concrete elements. In order to be suitable for standards and regulations, the method should be simple and practical enough to be used in engineering projects [7] [14]. Even though such models are developing and starting to be incorporated into design codes, most of the methods used to calculate shear capacity today are still based partly or entirely on empirical expressions instead of mechanical models [2] [14] [15]. The downside to using empirical expressions is that they are calibrated on the basis of available test data, and are therefore not always applicable to situations outside its calibration range. In these situations, empirical expressions could give inaccurate and potentially unsafe results [14].

The main objective of this study was to discover how a large axial load would affect the shear capacity in concrete beams without shear reinforcement. The results were then compared to the calculated values from two standards; Eurocode NS-EN 1992-1-1:2004+A1:2014 +NA:2018 (Eurocode 2) and DNVGL-ST-C502. As both of these standards have an empirical background in their shear calculations, it was also an objective to see how the equations would handle axial loads of large magnitudes.

A total of 9 shear-critical beams with different levels of axial loading were tested in a four-point loading system until failure. The first part of this paper will take a look at the theory of how axial compression affects the shear capacity in beams without transverse reinforcement, and how this is calculated in Eurocode 2 and DNVGL-ST-C502. The second part will focus on the experimental program by describing the materials and mechanical properties of the test beams, the set-up of the four-point test, and how the tests were monitored. In the third part, the experimental results will be presented and discussed, and compared to the calculations from the two standards.

2 Theoretical Shear Behaviour of Axially Loaded Concrete Beams without Shear Reinforcement

Shear fractures in concrete elements can be difficult to predict, even when applying advanced analytical programs. Combined with the brittle behaviour of concrete and the sudden development of a shear fracture, shear failure is one of the most dangerous types of concrete failure [18]. This is particularly true for members without shear reinforcement, as the deformation capacity is limited compared to members with transverse reinforcement [4]. To understand how the shear capacity can be affected by axial loading, one can look at the different types of shear failure and how the shear fractures typically develop.

2.1 Mechanical models

Due to the complexity and brittleness of shear failures, standards have used empirical expressions to calculate shear capacity for years. These expressions are usually calibrated on the basis of available test data from idealized academic testing, and are therefore limited in the sense that not all structures can be approximated by these tests. Another weakness of the expressions, is that their validity is limited to the load situations that were included in the calibration. Although these expressions have been improved by adding safety factors and correction factors to extend their range of use, it is starting to be acknowledged that design expressions in the standards

should be based on more adaptable mechanical models that describe the physical mechanisms behind shear failure [14] [10]. Suggested models include the Critical Shear Crack Theory, the Modified Compression Field Theory and the Multi-Action Shear Model, among others [10].

One of the best known mechanical models in this area is the Critical Shear Crack Theory (CSCT), which is the basis of the proposed shear design equations in the new version of Eurocode 2 [6] [14]. CSCT is based on the shear transfer mechanisms cantilever action, dowel action, aggregate interlock, residual tensile strength and arching action, and it assumes that the development of a critical shear crack will limit the strength of the member by disturbing these shear transfer actions [4] [6]. The shear transfer actions are explained in Appendix A. The theory states that the shear capacity depends on the geometry of the member, the strength of the concrete, and the width and roughness of the critical shear crack opening [4] [18].

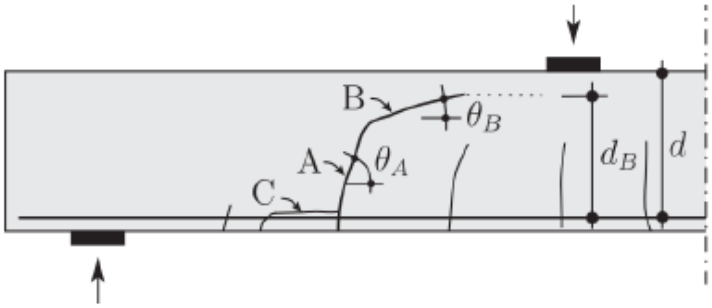

Figure 1: Crack development in a concrete beam [15].

Studies show a pattern in how shear cracks progress in a beam. The crack development is illustrated in Figure 1. Usually the shear crack begins in one of the vertical, flexural cracks that extend up to the longitudinal reinforcement. Above the reinforcement, the cracks are described by crack-types A-C [18].

A: A quasi-vertical part that develops at an angle Θ_A.

B: A quasi-horizontal part that develops at an angle Θ_B.

C: A delamination crack.

The length of each part can vary, but it is common for the quasi-vertical part to be bending induced. Therefore, this part extends up to the neutral axis, or to the fibre where the tension equals the tensile strength of concrete in bending. The origin of part B can be related to tensile stresses caused by beam shear-transferring actions [15].

The critical shear crack is defined as the crack with the design crack width, that eventually will cause the concrete to reach shear failure. However, it should be noted that the final failure surface may still end up with a different appearance than the critical shear crack, as it can be affected by other cracks during the failure process [2].

2.2 Types of Shear Failure in Beams without Shear Reinforcement

There are different types of shear failure for concrete beams. Inclined tension failure, shear compression failure and shear tension failure are considered as the most relevant for this project, as they are common failure types for beams without shear reinforcement, where the shear span to depth ratio is $a/d > 1$ [18]. Here, a is the distance between the point load and the support, and d is the distance from the top of the beam to the longitudinal reinforcement.

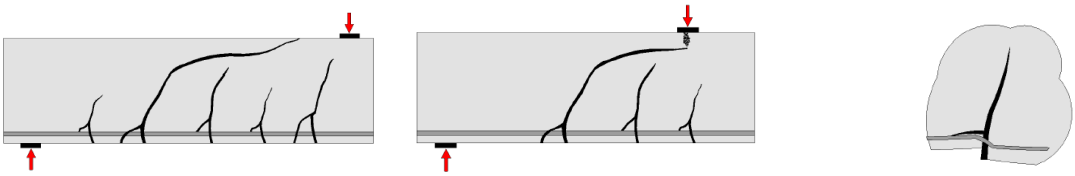

(a) Inclined tension failure. **(b)** Shear compression failure. **(c)** Delamination fracture can cause shear tension failure.

Figure 2: Types of shear failure in beams without transverse reinforcement. [18]

Inclined tension failure is illustrated in Figure 2a, and this failure type is common for beams with a shear span to depth ratio of $3 < a/d < 6$. The failure type is characterized by a diagonal shear crack continuing into the compression zone with a reduced inclination. It continues to propagate all the way through the compression zone. This occurs when the tension stress in the beam surpasses the tensile capacity of the concrete, and thereby causes brittle failure in the beam [18] [12].

A shear compression failure is illustrated in Figure 2b. This type of failure usually occurs when the shear span is shorter, $1 < a/d < 3$, and the shear crack is prevented from propagating through the entire compression zone of the beam. This might be caused by compression reinforcement, or the crack tip being underneath the point load. Eventually, cracks will develop in the compression zone due to large vertical compression stress, and the effective depth of the compression zone will be reduced. Failure is reached as the concrete underneath the shear load is crushed [12] [18].

As a shear crack develops, the concrete will experience a displacement in the vertical direction that will be prevented by forces from the longitudinal reinforcement (this dowel action is further explained in Appendix A). This can give cause to a delamination fracture, as illustrated in Figure 2c. Delamination fractures can cause the shear fracture to expand, and eventually prevent the longitudinal reinforcement from taking up tensile strain. The concrete will then reach shear tension failure, as concrete has a low ability to withstand tensile forces on its own [18].

2.3 Effect of Axial Compression

2.3.1 Axial Stress and Flexural Cracking

One way to explain how axial loading will affect the shear capacity of a concrete member, is to look at the moment, M_0, that will cause a flexural cracking pattern [18]. After flexural cracking have occurred, various shear-carrying mechanisms may induce tensile stress in the concrete. As tensile stress near the tips of the flexural cracks reaches the tensile strength of the concrete, the cracks will start to develop in a diagonal direction. From there, they may propagate and cause shear failure in the structure [16].

A specimen subjected to shear will always experience moment as well, as no member can have pure shear alone [12]. In a cross section subjected to axial force, shear force and moment, the normal stress will be evenly distributed, while the bending stress will have a linear distribution over the height of the cross section. The moment will cause compression in the top of the specimen, and tension in the bottom (or opposite, depending on the direction of the moment) [18] [17].

The compression stress from the axial force, σ_N, will counteract the tension stress from the moment, σ_M. As long as the compression stress is larger than the tension stress, flexural cracking will be prevented. At a certain magnitude of the moment, the tension in the bottom of the beam

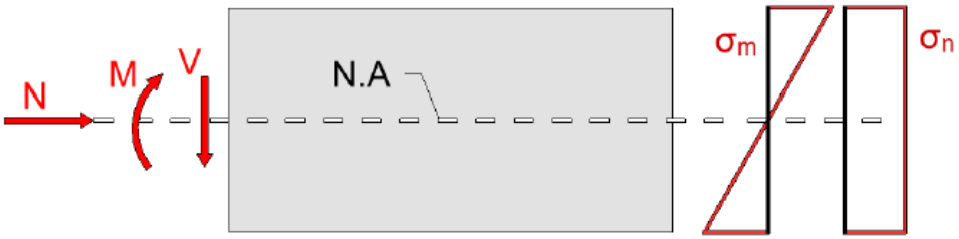

Figure 3: Stress caused by moment and axial forces [18]

will exceed the axial compression, resulting in tension in the bottom of the cross section. The bending stress that is necessary to counteract the axial stress is described in Equation 1. After the normal stress has been counteracted, flexural cracking is only prevented by the tensile strength of the concrete [17] [18].

$$\sigma_M - \sigma_N = 0 \tag{1}$$

In Equation 1, the stresses are defined as $\sigma_N = N/(bh)$ and $\sigma_M = M_0/W_c$. The normal stress depends on the axial force, N, the cross section width, b, and the cross section height, h. The bending stress depends on the counteracting moment, M_0, and the section modulus, W_c. This can be arranged to give an expression for the moment that is necessary to counteract the axial compression stress.

$$M_0 = \frac{NW_c}{bh} \tag{2}$$

As seen in Equation 2, increasing the normal force will have a direct impact on how large the moment needs to be in order to counteract the axial compression stress. A large normal force will increase the moment, and thereby increase the concrete's capacity against flexural cracking. As many shear failure cracks begin with a flexural crack, this will also increase the shear capacity [18].

2.3.2 Axial Stress and Shear Transferring Mechanisms

Shear transferring mechanisms are the different mechanisms or actions that contribute to the shear carrying capacity after flexural cracks have started to develop in the concrete. It should be noted that there are some differences in how researches describe these mechanisms, and to the level of importance that are placed on the different types [2] [15] [16].

The mechanisms are traditionally divided into two categories: beam shear-transfer actions and arching action. The beam shear-transfer actions consist of four different actions; residual tensile strength in the concrete, cantilever action, dowel action caused by the longitudinal reinforcement, and interface shear transfer caused by aggregate interlock. A combination of these beam shear-transfer actions and the arching action can almost always be used to describe the shear resistance in a concrete beam [4]. Factors like reinforcement ratio, concrete strength, size effect, span to depth ratio and axial force are considered to have significant influence on these mechanisms [12] [16]. All the shear-transfer actions are described in Appendix A.

As already mentioned, axial tensile stress will cause the concrete to have less resistance against shear failure, while axial compression stress will have the opposite effect. As the concrete is subjected to axial compression, the depth of the uncracked compression zone is increased, the tensile stress of the longitudinal reinforcement is reduced, and the width of the shear cracks decrease [12]. Consequently, the shear transfer in the compression zone and the aggregate

interlock action increase, resulting in a higher shear capacity [16]. The crack pattern will also be affected. When subjected to axial compression, the development of the critical shear crack happens at a lower angle and higher load level compared to members without axial compression [4]. This can change the failure pattern from inclined tension failure to shear compression failure [12].

3 Shear Capacity in Eurocode 2 and DNVGL-ST-C502

Calculating the effects of combined shear and axial loading is not a new topic, and it is reviewed in many standards and regulations. The standards Eurocode 2 and DNVGL-ST-C502 can be used to calculate how the shear capacity is affected by axial loading. Both of these standards have an empirical approach to calculating shear capacity in concrete beams without shear reinforcement [5] [9].

3.1 Shear Capacity in Eurocode 2

The Eurocode NS-EN 1992-1-1:2004+A1:2014+NA:2018 (Eurocode 2) is the reference design code for concrete structures in Europe [11]. In Eurocode 2, the method for finding shear capacity in concrete structures without shear reinforcement, is given by Equation 3 [5]. This is an empirical equation based on experimentation and testing of a number of different concrete members [17]. It combines empirical constants with the dimensions of the cross section, the material properties of the concrete, the amount of tensile reinforcement and the axial loading. Material- and safety factors are also included, in order to obtain a conservative result [5].

$$V_{Rd,c} = [C_{Rd,c}k(100\rho_l f_{ck})^{1/3} + k_1\sigma_{cp}]b_w d \tag{3}$$

The shear capacity, $V_{Rd,c}$, should have a minimum value of

$$V_{Rd,c} = (v_{min} + k_1\sigma_{cp})b_w d \tag{4}$$

In Equation 3, $C_{Rd,c}$ is a constant found in the national annex of Eurocode 2. It is set to $0.18/\gamma_c$ in the Norwegian annex, where γ_c is a safety factor of 1.5. The factor k should be equal to $k = 1 + \sqrt{\frac{200}{d}} \leq 2.0$, where d is the distance in mm from the top of the cross section to the centre of the reinforcement in the tension zone. ρ_l is calculated as $\rho_l = \frac{A_{sl}}{b_w d} \leq 0.02$, where A_{sl} is the cross-sectional area of the reinforcement in the tension zone, and b_w is the smallest width of the cross section in the tension zone. The characteristic compressive cylinder strength of the concrete after 28 days is represented by f_{ck}. Constants k_1 and v_{min} are also given in the national annex, and they are defined as $k_1 = 0.15$ and $v_{min} = 0.035k^{3/2}f_{ck}^{1/2}$ in the Norwegian version [5].

σ_{cp} is the stress in the concrete from axial loading due to external loads or prestressed reinforcement. This is the only factor that takes axial loading into account. It is set as $\sigma_{cp} = \frac{N_{Ed}}{Ac} < 0.2f_{cd}$, where N_{Ed} is the axial force. Here, the force is positive in compression and negative in tension, and A_c is the cross-sectional area of the concrete member. f_{cd} is the design value of f_{ck}, found by multiplying f_{ck} with the fraction α_{cc}/γ_c. α_{cc} takes long term effects and unfavorable application effects into account, and is set to 0.85 in the Norwegian annex. The limit value of $\sigma_{cp} < 0.2f_{cd}$ was set to avoid compression failure in the concrete [17].

It can be seen from the equation that the shear capacity, $V_{Rd,c}$, will increase with applied axial loading, N_{Ed}, as this will cause the stress, σ_{cp}, to increase. The shear capacity increases linearly with the axial force, until the stress reaches the limit value of $0.2f_{cd}$ where the shear capacity is considered to reach its maximum.

3.2 Shear Capacity in DNVGL-ST-C502

DNV GL is a classification society that provides a range of standards and regulations, giving a third party certification. The standard DNVGL-ST-C502 was developed to ensure a sufficient safety level for offshore concrete structures [8]. The DNV GL equation considering shear capacity of concrete structures without shear reinforcement, is given in Equation 5. This equation is also based on an empirical approach, and it uses many of the same factors as the equation from Eurocode 2 [9] [5].

$$V_{cd} = V_{co} + 0.8M_0\left|\frac{V_f}{M_f}\right| \leq \left(f_{td}k_v - \frac{0.25N_f}{A_c}\right)b_w z_1 \tag{5}$$

In Equation 5, M_0 is equal to $-N_f W_c/A_c$. W_c is the section modulus of the concrete cross section with respect to the extreme tension fibre or the fibre with the least compression, and A_c is the cross section area of the concrete member. N_f is the axial design load, and it is positive in tension. An axial compression force will therefore be described by a negative N_f, resulting in a positive M_0 and an increased shear capacity. V_f is the design shear force for the cross section under the considered conditions, and M_f is the total bending moment in the section acting in combination with the shear force, V_f.

A limit value for the shear capacity is found on the right side of the equation. Here, f_{td} is the design strength in uni-axial tension. The design tensile strength is expressed as $f_{td} = \alpha_t f_{tn}/\gamma_c$, where f_{tn} is the normalized tensile strength. This strength is defined as $f_{tn} = f_{tk}(1-(f_{tk}/25)^{0.6})$, where the characteristic tensile strength is given by $f_{tk} = 0.48(f_{cck})^{0.5}$. f_{cck} is the compressive cylinder strength of the concrete.

The factor k_v is set equal to $1.5 - d/d_1$, but should not be greater than 1.4 nor less than 1.0 for slabs and beams without shear reinforcement. d is the distance from the centre of the tensile reinforcement to the compression edge, and the distance d_1 is set to 1000 mm. Other factors that contribute to the shear capacity is the width of the beam, b_w, and the distance z_1 which is set as the greater of $0.7d$ and I_c/S_c. The moment of inertia for the uncracked concrete section is described by the factor I_c, and S_c gives the area moment about the centroid axis of the cross section for one part of the concrete section.

V_{co} in Equation 5 is the shear capacity in a concrete member without any coinciding axial force. This capacity is given by Equation 6.

$$V_{co} = 0.3\left(f_{td} + \frac{k_A A_s}{\gamma_c b_w d}\right)b_w d k_v \leq 0.6 f_{td} b_w d k_v \tag{6}$$

In Equation 6, A_s is the cross-sectional area of properly anchored reinforcement on the tension side, γ_c is a material factor for concrete and the factor k_A is set to 100 MPa.

The calculated shear capacity from Equation 5 will increase linearly with the axial force. In order to prevent compression failure, the limit is set at the point where N_f/A_c reaches a numerical value of $0.4f_{cd}$ [9].

4 Experimental Program

The experimental program was designed to find the shear capacity in axially loaded concrete beams without shear reinforcement. Nine simply supported beams were tested in a four-point loading system, as illustrated in Figure 4. The four-point test ensured that the spans between the supports and the applied loads were evenly subjected to shear force, as shown in Figure 5 with a corresponding moment diagram shown in Figure 6.

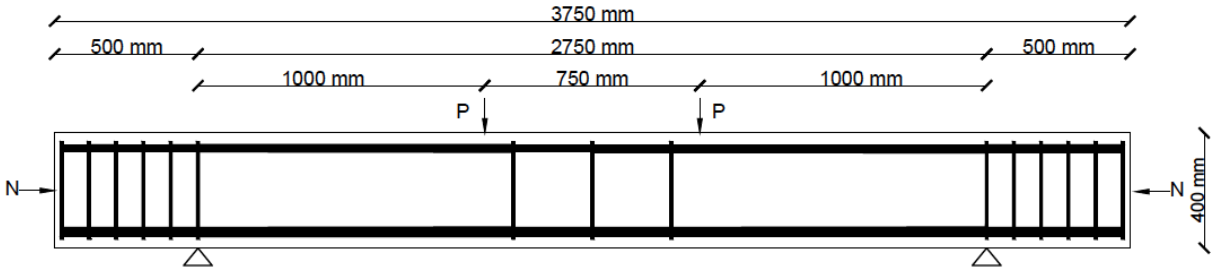

Figure 4: Longitudinal section of the simply supported beam, showing the reinforcement and where the shear forces (P) and axial forces (N) were applied during the test.

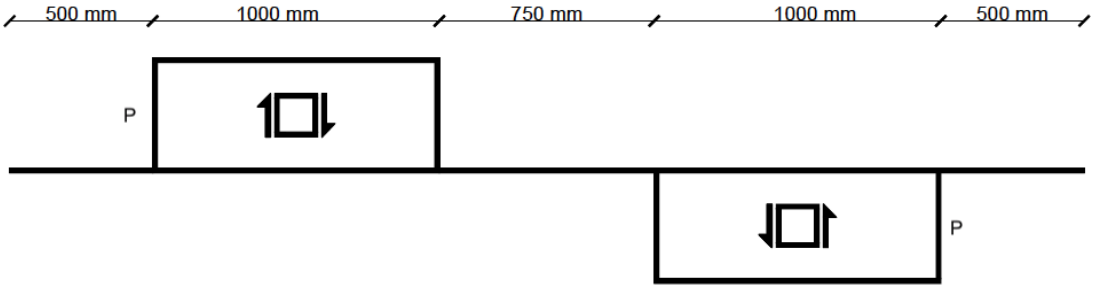

Figure 5: Shear force diagram of the simply supported beam.

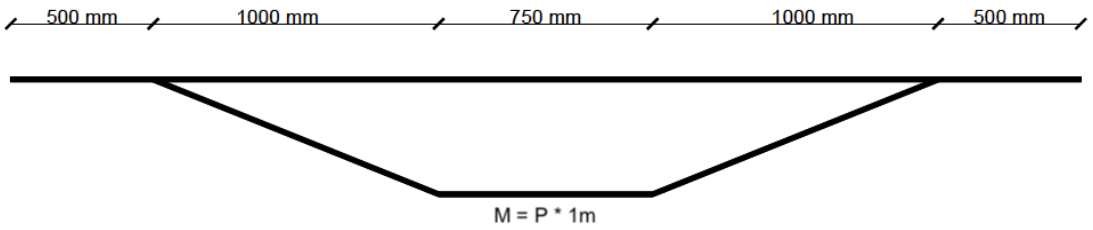

Figure 6: Moment diagram of the simply supported beam.

The test beams were labeled with the descriptive letter B, followed by numbers from 1 to 9. They were then separated into three sets, where the first set (B1-B3) was considered as a reference set, to be tested without any applied axial force. The beams in the second set (B4-B6) were loaded with an axial force of 500 kN, and the beams in the third set (B7-B9) were loaded with an axial force of 800 kN.

4.1 Test Beams

4.1.1 Beam Geometry and Reinforcement

All the beams in the study were identically manufactured, with a 400 mm high and 250 mm wide rectangular cross section as illustrated in Figure 7. Each beam had a total length of 3750 mm, with the supports placed symmetrically, 2750 mm apart. The point loads were applied 750 mm apart, giving each shear span a length of 1000 mm.

During the four-point loading test, the central part of the beam would be subjected to pure bending (as shown in Figure 6). To increase the moment capacity and thereby ensure that the beams would become shear-critical, the test beams were reinforced with two bars with a diameter

of 25 mm in the compression zone, and three bars with a diameter of 32 mm in the tension zone.

Three 10 mm stirrups were included as transverse reinforcement in the central part of the beam, in order to prevent buckling of the top reinforcement bars. They were placed symmetrically with a spacing of 275 mm. In order to secure sufficient anchoring of the reinforcement bars, six stirrups were also placed on the outside of each support. The concrete cover was 30 mm on the top and bottom of the beam, and 20 mm on the sides. The beams were free from any transverse reinforcement in the shear spans, so that the results would be valid for concrete beams without shear reinforcement. All the reinforcement is shown in Figure 4 and 7.

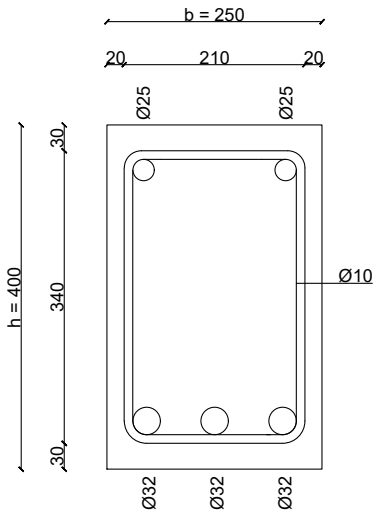

Figure 7: Cross section. All measurements are in millimetres

4.1.2 Materials and Mix Proportions

The project aimed for a concrete with a mean compressive strength of 35 MPa, using the concrete mixture composition shown in Table 1. The concrete was produced externally and cast into formwork at Contiga's factory in Fredrikstad. The formwork was constructed as a wall formwork, meaning that the beams had to be cast horizontally. Vibrating the concrete in a horizontally lying formwork could have resulted in a higher concentration of aggregate at the bottom of the formwork, making the beam strength unsymmetrical [1]. A self-compacting concrete was therefore chosen, to be able to avoid compacting the concrete by vibration.

Constituent	Weight [kg/m^3]
Sand 0/8	1102
Gravel 8/16	660
Standard cement FA	270
Industrial cement	116
Water	175
Super plasticizer (77% water)	4.452
Air entraining agent (80% water)	0.774

Table 1: Concrete mixture composition of the test beams.

4.1.3 Mechanical Properties

As the same formwork was used for all the beams, only one beam could be made per day. Consequently, it was not possible to use the same concrete mix batch in all the beams. As a result there could be small variations in the concrete properties and beam strengths, even though all beams used the same concrete recipe. To determine the concrete properties, three cubes were cast along with each beam, using concrete from the same batch as the beam. The average strength of these cubes would give a more accurate estimation of the concrete strength in each beam.

The beams were wrapped in wet fabric and plastic during the curing process, and the cubes were stored in water. Both beams and cubes were stored inside for more than 28 days before testing, to ensure that the mechanical properties would be as stable as possible.

As the strength of concrete changes during the curing process, the concrete cubes were meant to be tested the same day as the testing of the corresponding beams. However, due to limited staff during the COVID-19 pandemic, it turned out that the DNV GL lab did not have the capacity to test the concrete cubes. All the cubes were therefore sent to a different laboratory, and they were all tested on the same day (4-13 days after the testing of the corresponding beams). This delay may have caused a higher estimate of the concrete strength. Still, any increase of the concrete strength should be limited, as all testing was conducted more than 28 days after manufacturing, and the development of concrete strength is less significant after the first 28 days.

No.	Cast date	Test date	Average $f_{c,cube}$	Average f_c
B1	02.03	01.04	68.2	54.6
B2	06.03	08.04	54.8	43.8
B3	12.03	10.04	55.7	44.6
B4	03.03	02.04	61.7	49.4
B5	10.03	09.04	55.2	44.2
B6	11.03	10.04	55.7	44.6
B7	04.04	03.03	58.2	46.6
B8	05.03	08.04	59.0	47.2
B9	09.03	09.04	62.8	50.2

Table 2: Average cube and cylinder strength for beams B1-B9.

Another consequence of the virus outbreak, was that the three last cubes did not get produced. The strength of the corresponding beam, beam B3, was therefore set as equal to the strength of beam B6, as these beams were tested on the same day and cast only a day apart.

The average strengths from the cube testing are given in Table 2. In order to convert the average compressive cube strength, $f_{c,cube}$, to cylinder strength, the formula $f_c = 0.82 * f_{c,cube}$ from Eurocode 2 was used [5]. Even though the factors for concrete strength are described by different symbols in DNVGL-ST-C502 (f_c for cube strength and f_{cc} for cylinder strength), the Eurocode notations will be used in the remainder of this paper to avoid confusion.

The average cylinder strength of all the 27 test cubes were $f_{c,average} = 48.4MPa$.

4.2 Set-up

A mechanical jack was used to apply the axial force to the beams before the four-point test started. When applying the axial force, steel plates were used to distribute the force uniformly over the entire cross section on each side of the beam. The force was applied in the center of the steel plates, to allow rotational freedom. Ideally, these steel plates should be completely free to

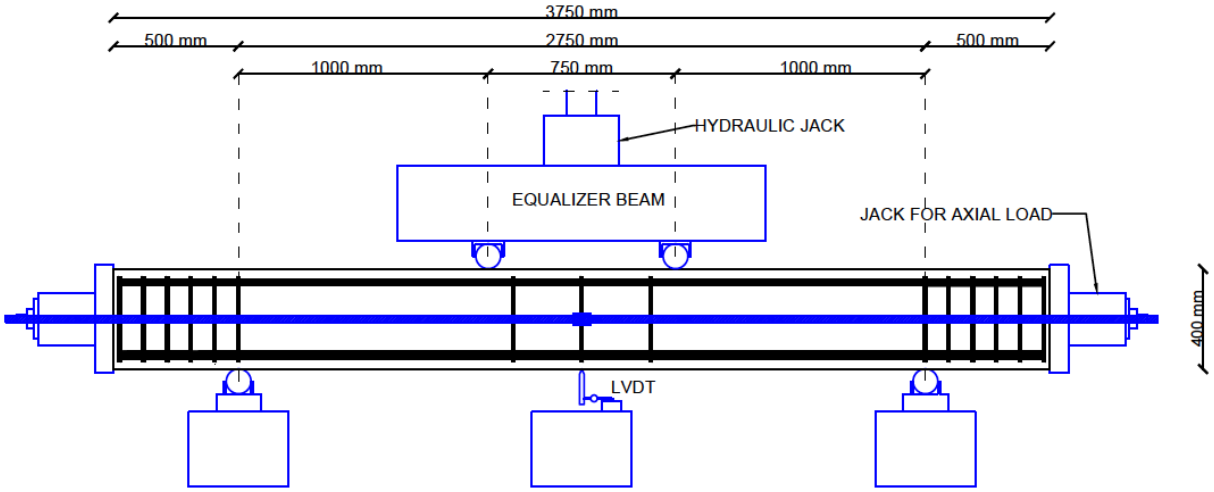

Figure 8: Set-up of the four-point test with hydraulic jack to apply shear force, mechanical jack for axial load and LVDT to measure displacement under the beam in the midspan.

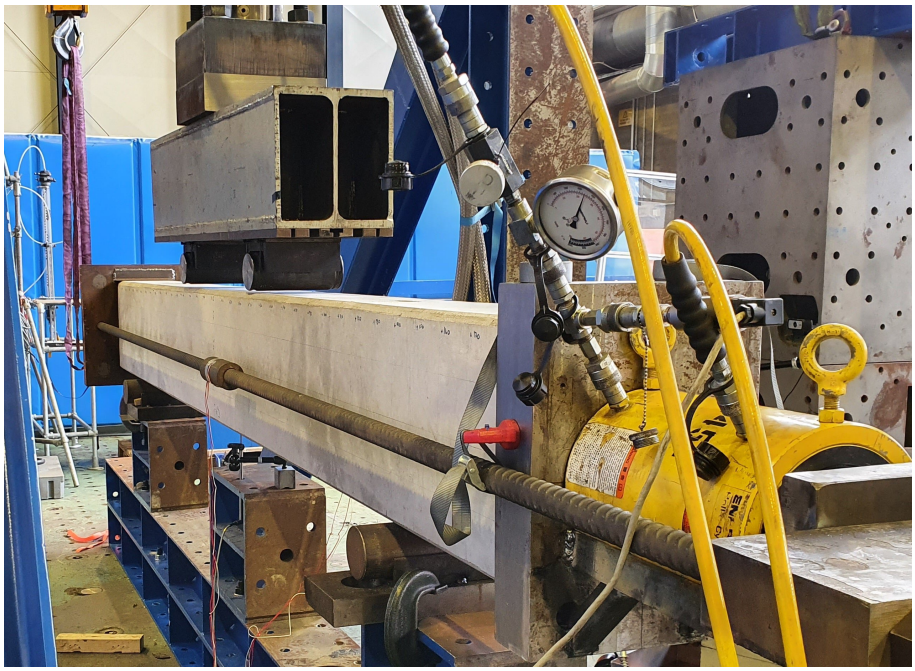

Figure 9: Complete set-up of the four-point test on an axially loaded beam.

rotate during the four-point test, but in reality this can be difficult to achieve. A small restraining effect may therefore have affected the moment- and shear distribution and the deflection during testing. The application of the axial force may also have resulted in an eccentricity moment that increases with increasing deflection, as the direction of the axial force would not change with the beams when they started to deform vertically. However, by applying the normal force externally, an accurate measure of the axial load could be made during the course of the test. Measuring the exact axial force would be much more difficult in prestressed beams, due to e.g. tension loss in the prestressing strands. A close-up of the applied axial load is shown Figure 10.

Figure 10: The axial load was applied using a jack and steel plates.

After applying the axial load, the four-point test was started. It was conducted using a hydraulic jack, where the force from the jack was distributed to two point loads by using an equalizer beam with two roller supports. The four-point test was displacement controlled, with a loading rate of 0.5 mm/min. The complete set-up is illustrated in Figure 8 and pictured in Figure 9.

4.3 Instrumentation

The tests were instrumented to measure the applied axial force, the applied shear force, and the displacement in the middle of the beam. To maintain a displacement controlled test, the displacement of the hydraulic jack piston was controlled through an actuator. The magnitude of the applied shear and axial forces were monitored by a load cell on the piston of the hydraulic and mechanical jack, respectively. In order to find the magnitude of each point load, the applied load was divided by two. A linear variable differential transformer (LVDT) was placed underneath the middle of the beam, to measure the vertical beam displacement during testing. Both displacement and load readings were logged with a rate of 5 Hz. Pictures were also taken of the front and back of the two shear spans in the beams, every 4th second during the four-point test.

5 Results

All the beams reached shear failure during testing, and pictures of the shear failure cracks are given in Appendix C. By using the measured shear load and displacement, load-displacement relationships could be plotted for each beam. The graphs were then adjusted to account for flexibility of the support of the beams. The resulting load-displacement graphs are presented in Figure 11 for beams B1-B3, in Figure 12 for beams B4-B6, and in Figure 13 for beams B7-B9. All the individual graphs are given in Figure 14.

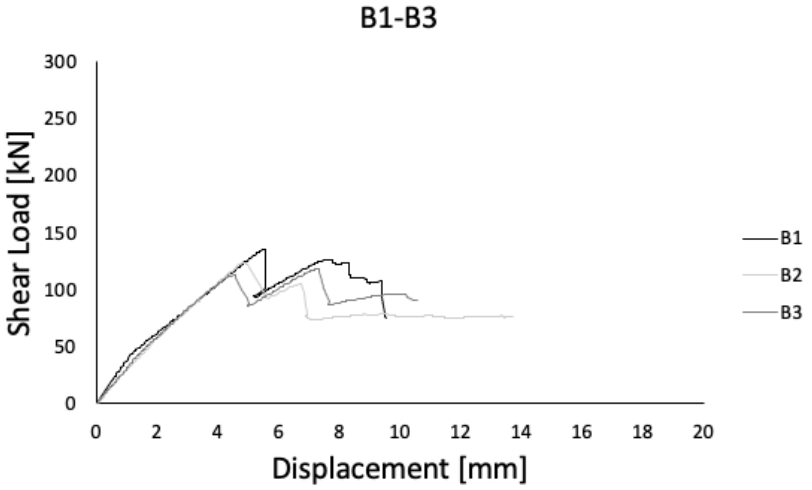

Figure 11: Load-displacement relationship for beams B1-B3 without any axial load.

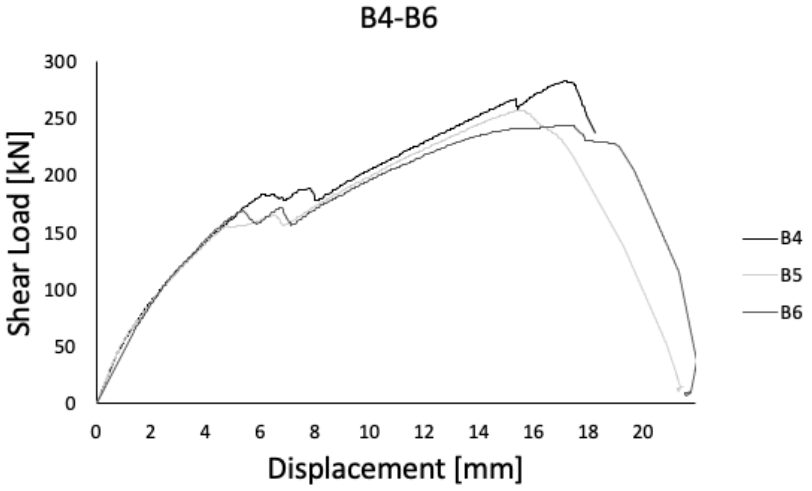

Figure 12: Load-displacement relationship for beams B4-B6 with an axial load of 500 kN.

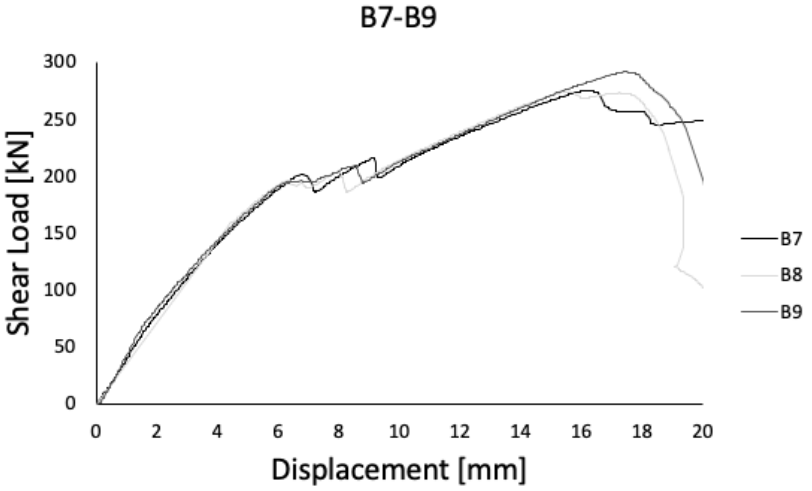

Figure 13: Load-displacement relationship for beams B7-B9 with an axial load of 800 kN.

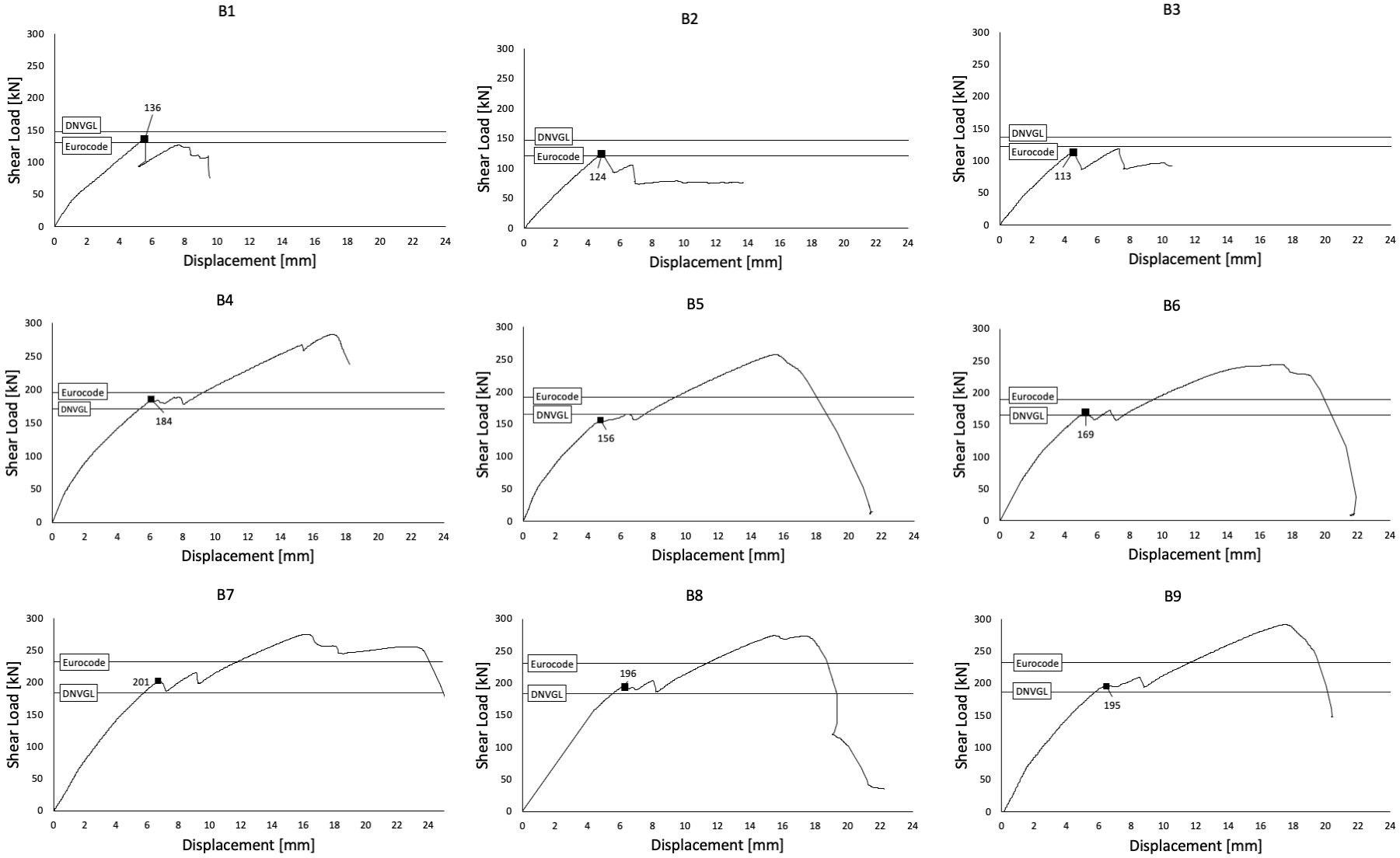

Figure 14: Load-displacement diagrams for beams B1-B9, with calculated capacities found in Eurocode 2 and DNVGL-ST-C502.

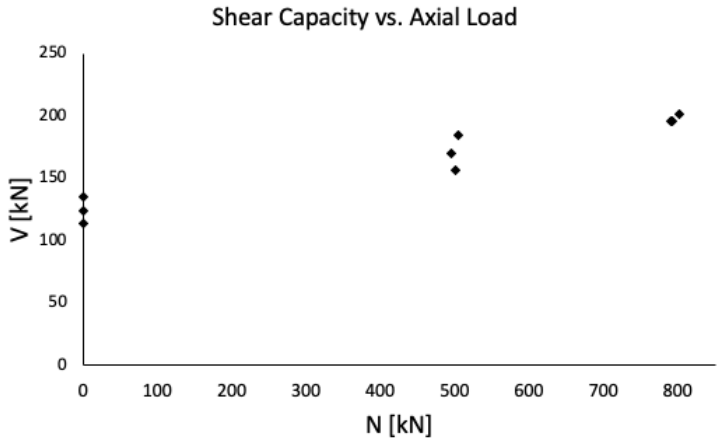

Figure 15: Observed shear capacity and axial load at failure for the 9 test beams.

By defining failure at the first peak the in load-displacement graphs, the shear capacities of the beams could be plotted with the measured axial load at the moment of failure. The resulting scatter plot is shown in Figure 15. These results are also given in Table 3, along with the measured displacement of the beams.

In Table 3, the shear capacity of each beam is compared to the calculated values from DNVGL-ST-C502 and Eurocode 2. These shear capacities were calculated by omitting all safety- and material factors from the equations, and by using the measured axial load at failure. Additionally, the concrete strengths from Table 2 were used instead of the characteristic concrete strengths. This was done to get a better picture of the underlying accuracy of the expressions in the standards. The calculated shear capacities were also plotted into the shear-displacement graph for each beam in Figure 14. It should be noted that if characteristic strengths were used and all material- and safety factors were applied, the calculations would have been much more conservative.

No.	Axial load	Shear capacity	Shear capacity Eurocode 2	Shear capacity DNVGL-ST-C502	Displacement
B1	0 kN	136 kN	131 kN	147 kN	5.5 mm
B2	0 kN	124 kN	122 kN	136 kN	4.9 mm
B3	0 kN	113 kN	123 kN	137 kN	4.5 mm
B4	505 kN	184 kN	192 kN	169 kN	6.1 mm
B5	501 kN	156 kN	187 kN	163 kN	4.8 mm
B6	495 kN	169 kN	187 kN	163 kN	5.3 mm
B7	802 kN	201 kN	228 kN	182 kN	6.7 mm
B8	792 kN	196 kN	227 kN	182 kN	6.3 mm
B9	790 kN	195 kN	230 kN	185 kN	6.5 mm

Table 3: The observed and calculated shear capacity for the test beams B1-B9, including the axial load and displacement at failure.

6 Discussion

6.1 Failure Modes

The load-displacement graphs (see Figure 14) were used to find the shear capacity of each beam. For beams B1-B3, these graphs showed a peak followed by a sudden drop. This first peak was considered to mark failure, and would give the beam's shear capacity. Checking the pictures from testing confirmed the same; at the time of the first drop, a defined shear crack appeared in the pictures. After the drop, the graph proceeded to rise once again, showing some post-failure capacity before collapse.

For the beams with axial load, the graphs were not as self-explanatory (see Figure 12 and 13). The first shear crack discovered during testing, showed up in the graph as more of a jagged plateau than a sudden drop after the first peak. Initially, the fracture was not very prominent in the pictures. However, the initial shear crack development was similar to what was seen for B1-B3, where a sudden shear crack propagation was observed, followed by a slow expansion of the crack width. The first peak in the graph was therefore considered as the point of failure. In the beams with axial loading, the graph would continue to rise significantly after the first shear fracture, showing a post-failure strength about $40\% - 50\%$ higher than the shear capacity. Finally, the beams would reach a second peak. At this stage, the graph would suddenly drop, and the pictures showed an explosive collapse of the beam. Pictures of the crack development for B9 are shown in Figure 16, 17 and 18, as an example of the crack development in beams B4-B9.

Beams B4-B9 showed significant post-failure shear capacities. One reason for this, could be the test set-up. A consequence of using a displacement controlled procedure during testing, is that there will be a temporary reduction in the applied shear load when a beam has a sudden deformation due to crack development. This temporary reduction might help the forces in the beam to be redistributed, preventing the beam from collapsing. The beams will therefore be more likely to obtain a post-failure capacity. This is less likely to happen outside of the lab, where the applied loads are usually not temporarily reduced as the concrete deforms. Hence, the capacity found in the second peak during testing could be less significant in reality.

As only the beams with applied axial load had large post-failure capacities, the axial load seems to contribute significantly. This could be because the axial load helps with the redistribution of forces, but it could also be because of the axial compression force itself. In order to assess how the axial load affects post-failure capacity, a load controlled test could be better suited than a displacement controlled test. A load controlled test will try to keep a constant load rate, giving less of a reduction in the force as the concrete starts to deform, and the redistribution effect in the test beams would therefore be reduced. If the beams still obtained large post-failure capacities in load controlled testing, it would imply that the axial compression also had an effect on its own, regardless of any redistribution of forces in the beam.

As a control check, the flexural cracking load was calculated. The calculations are shown in Appendix B. The load should be around 35 kN for B1-B3, around 70 kN for B4-B6 and around 90 kN for B7-B9. These values correspond well with small bends in the load-displacement graphs (especially visible for B1, B5 and B9 in Figure 14), suggesting that flexural cracking occurred at these points. These bends were expected at the flexural cracking loads, as the bending stiffness will be reduced when the concrete transitions from uncracked to cracked stage, resulting in a reduced inclination of the load-displacement graph [17]. Even so, no flexural cracking was visible in the photos, suggesting that smaller cracks were in general difficult to detect during the test. This supports the decision of defining the first peak in the load-displacement graph as the point of failure, in spite of the moderate appearance of the failure crack in the pictures.

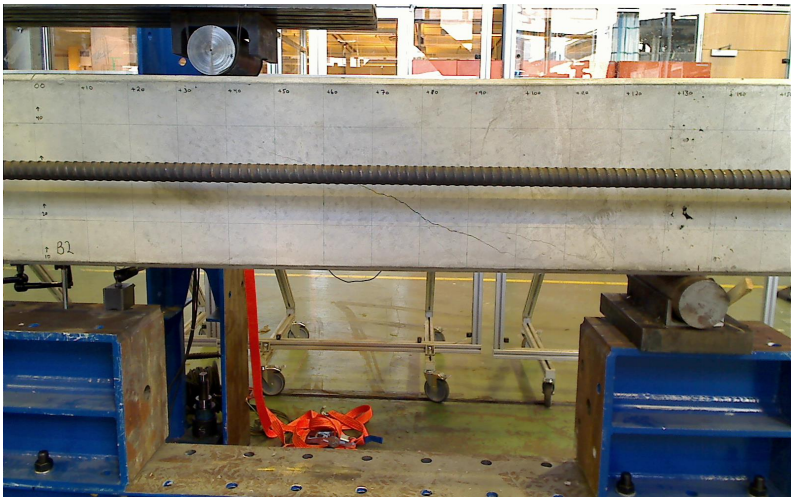

Figure 16: Initial shear crack in B9 that appeared after the first peak in the shear-displacement graph.

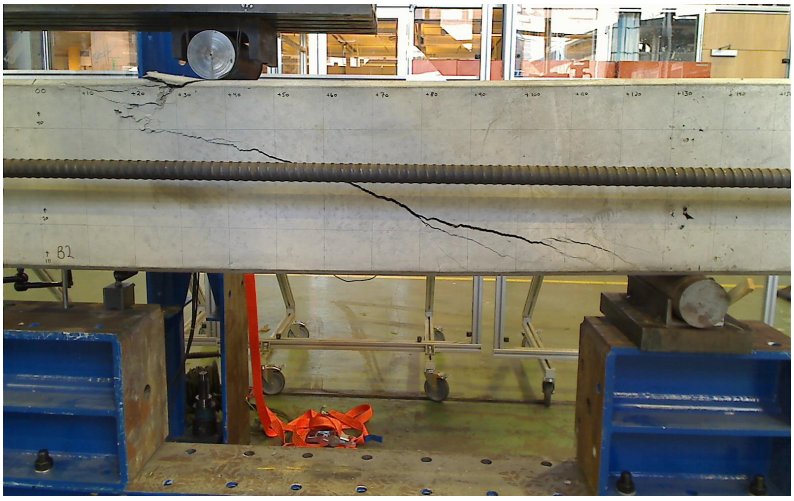

Figure 17: The initial crack in B9 developed further towards the second peak in the shear-displacement graph.

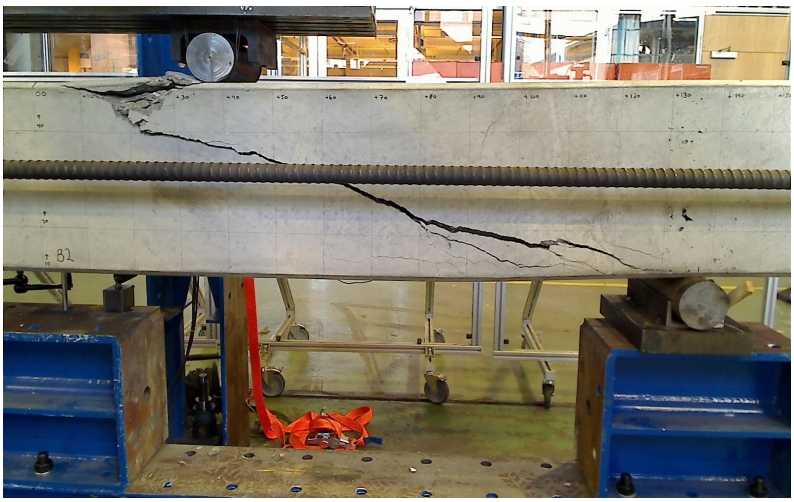

Figure 18: Picture taken after the second peak in the shear-displacement graph for B9.

Pictures of all the failure modes are given in Appendix D. The pictures are taken around the time of the first and second peak in the load-displacement graph for each beam, showing the point of failure and collapse. For the beams with axial load, a picture taken just before the second peak was also included, to better show the shape of the initial shear failure crack. The failure development between the first and second peaks was mainly widening of the shear crack that occurred at the first peak. It was noted that beams B1-B3 (without axial load) seemed to have reached inclined tension failure, where the crack propagated through the entire compression zone of the beam, at close to 45°. The beams B4-B9 had failure cracks with lower inclination and crushing of the concrete below the point load, suggesting shear compression failure. It should also be noted that some beams showed a clear redistribution of forces after initial failure, where delamination fractures along the bottom reinforcement bars were observed, followed by a new shear crack appearing at a steeper angle.

6.2 Displacement

The bending deflection was calculated at the midspan of the beam, neglecting the contribution from shear [17]. It was calculated in the serviceability limit state, before and after flexural cracking, and the calculations are shown in Appendix: B. The calculation model assumes that both concrete in compression and reinforcement steel are linear and elastic materials, following Hooke's law. This gives $\sigma_c = E_{cm}\varepsilon_c$ and $\sigma_s = E_s\varepsilon_s$. The model also assumes that concrete has zero tensile strength, and it incorporates Navier/Bernoulli's hypothesis that plane sections remain plane and normal to the longitudinal axis after bending [17]. The deflection formula for the simply supported test beams is based on the relationship between deflection and moment from Euler-Bernoulli beam theory:

$$M = -EI\frac{d^2w}{dx^2} \tag{7}$$

By using the method of double integration, the maximum deflection at the midspan of the beam is given by Equation 8. Here, the factor P is the point load, L is the length of the beam between the supports, and a is the distance between the supports and the point loads. The bending stiffness EI will change as the concrete transitions from the uncracked stage to the cracked stage. The final displacement was found by adding both contributions.

$$\delta = \frac{Pa}{24EI}(3L^2 - 2a^2) \tag{8}$$

Uncracked stage

At the uncracked stage, the compression zone depth is:

$$\alpha d = \frac{A_c \cdot 0.5h + \eta A_s d}{A_c + \eta A_s} \tag{9}$$

where $\eta = E_s/E_{cm}$. The moment of inertia of the concrete and reinforcement steel are given by:

$$I_{c1} = \frac{bh^3}{12} + bh(\alpha d - \frac{h}{2})^2 \quad , \quad I_{s1} = A_s(d - \alpha d)^2 \tag{10}$$

The bending stiffness for the uncracked stage is:

$$(EI)_1 = E_{cm}I_{c1} + E_sI_{s1} \tag{11}$$

Cracked stage
For cracked concrete, the compression zone depth is given by:

$$\alpha = \sqrt{(\eta\rho)^2 + 2\eta\rho} - \eta\rho \tag{12}$$

where $\rho = A_s/(bd)$. The moment of inertia of the concrete is given by:

$$I_{c2} = \frac{1}{2}\alpha^2(1 - \frac{\alpha}{3})bd^3 \tag{13}$$

Then the bending stiffness for the cracked stage can be calculated by:

$$(EI)_2 = E_{cm}I_{c2} \tag{14}$$

No.	Observed displacement	Calculated displacement	Reinforcement tension at 50% of failure load
B1	5.5 mm	5.4 mm	95 MPa
B2	4.9 mm	5.1 mm	87 MPa
B3	4.5 mm	4.7 mm	80 MPa
B4	6.1 mm	7.5 mm	130 MPa
B5	4.8 mm	6.4 mm	110 MPa
B6	5.3 mm	7.0 mm	119 MPa
B7	6.7 mm	8.2 mm	142 MPa
B8	6.3 mm	8.0 mm	138 MPa
B9	6.5 mm	7.9 mm	137 MPa

Table 4: The observed and calculated displacement in the middle of beams B1-B9 at failure, as well as the reinforcement stress at 50 % of the failure load

The calculated displacements are compared to the observed displacements in Table 4. As a control check, the tension in the reinforcement was calculated for 50% of the failure load for each beam.

$$\sigma_s = E_s\frac{M \cdot (1-\alpha)d}{(EI)_2} \tag{15}$$

All results are shown in Table 4. The results show that the reinforcement will not yield before failure. This means that the assumptions for the displacement calculations are applicable, and that the calculations should be quite accurate.

The beams with axial load experienced lower deflection than calculated, illustrating an effect from the axial load. As the axial load will increase the flexural cracking moment, the concrete will remain in the uncracked stage for a longer amount of time. The concrete in the uncracked stage has a larger bending stiffness, and the deflection will thereby be reduced.

6.3 Calculated and Observed Shear Capacity

The results from the four-point testing show that the shear capacity in the test beams increased when subjected to axial loads of large magnitude. On average, the shear capacity increased by 37% and 59% when the axial compression load was 500 kN and 800 kN, respectively. As shown

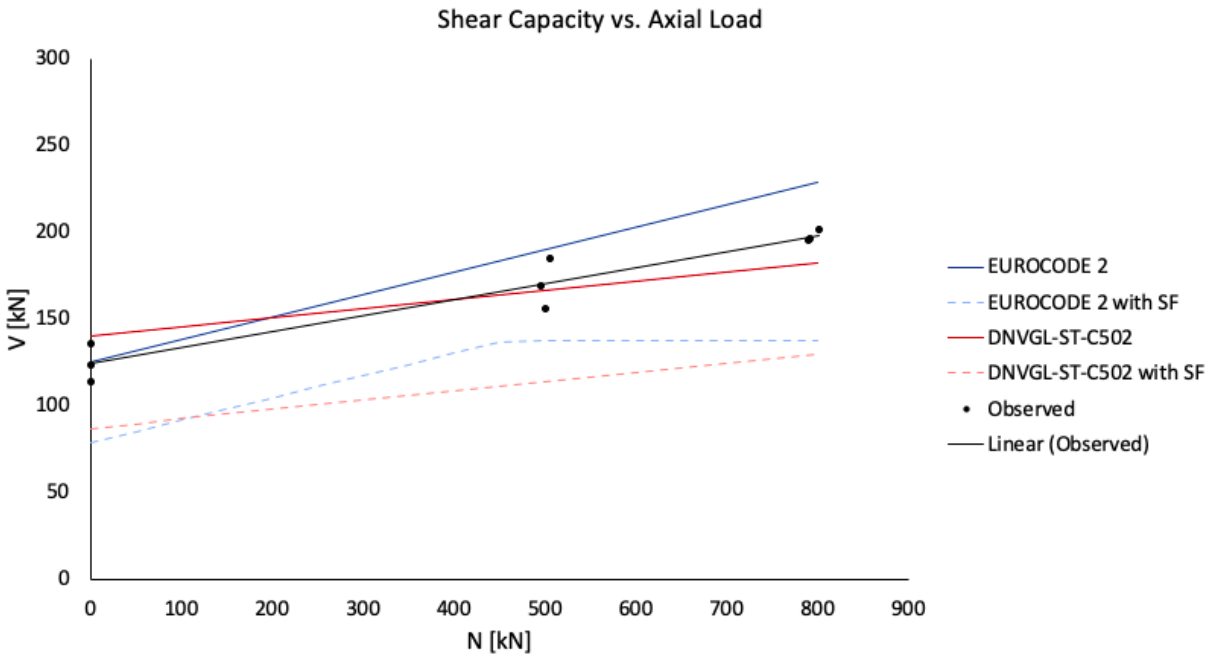

Figure 19: Shear Capacity from Eurocode 2 and DNVGL-ST-C502, with and without safety factors (SF), compared to the observed capacities of the beams.

in Figure 19, the observed shear capacity and axial load of the test beams could fit well with a linear trend line, illustrating how the shear capacity increases with increasing axial compression. The standard error of the trendline was 9.6 kN for the shear capacity.

The calculated shear capacities from Eurocode 2 and DNVGL-ST-C502 were also plotted in Figure 19. The graphs were calculated by using the average concrete strength of the test beams instead of characteristic strength, and by omitting all safety and material factors. The resulting graphs would therefore give a better picture of the underlying accuracy of the standards. Additionally, the capacities were calculated with all safety and material factors as well as characteristic strengths, to illustrate the safety of the equations as they are used in engineering projects. These graphs are shown with dashed lines in Figure 19.

The calculated shear capacity from the Eurocode 2 seems to be quite accurate for the beams without axial loading. However, as the axial load is applied, the graph grows with a steeper slope than the trendline from the observed shear capacity. As the axial loading reaches larger magnitudes, the calculated capacity from the Eurocode moves further away from the observed results. At axial loads of 500 kN and 800 kN, the calculated capacity from Eurocode 2 is 12% and 15% higher than the observed trendline, respectively. Thus, the calculations were giving unsafe results for high axial loads, when using the average concrete strength and omitting material and safety factors. The increasing inaccuracy was also observed in the individual load-displacement graphs in Figure 14. Even though the results will be on the safe side when characteristic strength and safety factors are included, this indicates that the Eurocode overestimates the effect of axial load on shear capacity.

The shear capacity graph based on DNVGL-ST-C502 exceeds the observed trendline with 13% for the beams without axial load. Hence, when omitting safety factors and using average concrete strength, the DNV GL calcuations give unsafe results for beams that are only subjected to shear loads. However, the graph has a gentle slope as the axial load increases, and the DNV GL capacity crosses over to the safe side of the trendline when the axial load reaches about 400

kN. Despite the calculated value being high for beams without axial load, the results at $N = 500$ kN and $N = 800$ kN are more accurate than the calculations from the Eurocode 2. This implies that DNVGL-ST-C502 underestimates the effect of the axial load on the shear capacity.

It should be noted that Eurocode 2 has an upper limit to avoid compression failure at $\sigma_{cp} < 0.2 f_{cd}$. The upper limit in DNVGL-ST-C502 is given by $N_f/A_c = 0.4 f_{cd}$. When using average concrete strength and omitting safety factors, the calculated capacity graph for Eurocode 2 will therefore reach its maximum at an axial load of 1000 kN, with a coinciding shear capacity of 250 kN. The DNV GL graph will reach this point when the axial load is 1950 kN, giving a maximum shear capacity of 243 kN for the test beams. While the maximum shear capacities are almost the same in both standards, the DNVGL-ST-C502 allows almost twice as large axial load before the maximum shear capacity is reached.

On the basis of the results from this project, it is recommended to do further studies on the shear capacity formulas in both standards, especially the terms including the axial force, to see if the factors are correctly calibrated or if they can be improved. It is also recommended doing research on beams subjected to even higher axial loads, in order to examine the behaviour of beams approaching the compression failure limits and the corresponding maximum shear capacities found in the standards.

7 Conclusion

This study concludes that the shear capacity in beams without shear reinforcement increases when the bears are subjected to axial loads of large magnitude. On average, the shear capacity increased by 37% and 59% when the axial compression load was set to 500 kN and 800 kN, respectively. The relationship between the axial load and the shear capacity could be seen as linear. All nine test beams experienced shear failure during testing. The beams without axial load developed inclined shear tension failure, and the beams subjected to axial load developed shear compression failure.

Both the Eurocode 2 and the DNVGL-ST-C502 assume a linear relationship between applied axial load and shear capacity. While Eurocode 2 gives quite accurate results for the beams without axial loading, the calculated shear capacity exceeds the observed capacity for the beams with axial loads of 500 kN and 800 kN. The results from DNVGL-ST-C502 exceed the observed values for the beams without axial loading, but has a more gentle increase in the shear capacity when the axial loading increases, resulting in a more accurate result for beams B4-B9 with high axial load. The results are based on calculations without any material- or safety factors, and with average concrete strength instead of characteristic strength. If all factors were included and the characteristic strengths were used, the calculated capacities from both standards would be conservative. Even so, the results still indicate that the Eurocode overestimates the effect of axial compression on the shear capacity, and that the effect is underestimated by DNVGL-ST-C502. It is therefore recommended to do further studies on these shear capacity formulas, especially the terms including the axial force, to see if the factors here are correctly calibrated or if they can be improved.

8 Acknowledgements

The authors would like to acknowledge the assistance of R. Fosse and the staff at DNV GL laboratory in Høvik for performing the lab testing, in addition to the financial support from DNV GL for the production of the test beams. Acknowledgements are also made to Contiga and Thomas Andersen for producing the beams, and to Statens Vegvesen and Erik Sveen for testing the concrete cubes.

References

[1] Baláz *et al.* (2009) *Structural Concrete - Textbook on behaviour, design and performance*. fib, Lausanne.

[2] Cavagnis, F., Ruiz, M.F. and Muttoni, A. (2015) Shear failures in reinforced concrete members without transverse reinforcement: An analysis of the critical shear crack development on the basis of test results, *Engineering Structures*, vol. 103, p. 157–173. https://www.sciencedirect.com/science/article/abs/pii/S0141029615005787

[3] Cavagnis, F, Ruiz, M.F. and Muttoni, A. (2017) An analysis of the shear-transfer actions in reinforced concrete members without transverse reinforcement based on refined experimental measurements, *Structural concrete*, vol. 19, nr. 1, p. 1-16. https://www.researchgate.net/publication/321427260_An_analysis_of_the_shear-transfer_actions_in_reinforced_concrete_members_without_transverse_reinforcement_based_on_refined_experimental_measurements

[4] Cavagnis, F. (2017) *Shear in reinforced concrete without transverse reinforcement: from refined experimental measurements to mechanical models*. PhD thesis. École Polytechnique Fédérale de Lausanne.

[5] CEN European Committee for Standardization (2014) *NS-EN 1992-1-1:2004+A1:2014+NA:2018: Eurocode 2: Design of concrete structures - Part 1-1: General rules and rules for buildings*

[6] CEN European Committee for Standardization (2017) *prEN1992-1-1:2017, Draft of Eurocode 2: Design of concrete structures Part 1–1: General rules and rules for buildings, bridges and civil engineering structures*

[7] De Wilder, K. *et al.* (2015) 'Experimental investigation on the shear capacity of prestressed concrete beams using digital image correlation', *Engineering Structures*, Volume 82, p. 82-92 https://www.sciencedirect.com/science/article/pii/S0141029614006397

[8] DNV GL, 'About us', https://www.dnvgl.com/about/index.html

[9] DNV GL (2018) *DNVGL-ST-C502 Offshore concrete structures*

[10] International Federation for Structural Concrete. (2018) *Towards a rational understanding of shear in beams and slabs*. (Fib Bulletin no. 85). Fib, https://www.fib-international.org/publications/fib-bulletins/towards-a-rational-understanding-of-shear-in-beams-and-slabs-pdf-detail.html

[11] European Comission Joint Research Centre, 'About the EN Eurocodes', https://eurocodes.jrc.ec.europa.eu/showpage.php?id=1

[12] Gou, Z. (2014) *Principles of Reinforced Concrete*, E-book, p. 349-384, https://www.sciencedirect.com/science/article/pii/B9780128008591000141#s0125

[13] Jørgensen, H.B. *et al.* (2013) Influence of High Axial Tension on the Shear Strength of non-shear RC Beams, *Proceedings of the International IABSE conference: Assessment, Upgrading, Refurbishment of Infrastructures*, Rotterdam, 06.05.13-08.05.13, https://backend.orbit.dtu.dk/ws/portalfiles/portal/87525198/IABSE_Paper_2013.pdf

[14] Muttoni, A. and Ruiz, M.F. (2019) From experimental evidence to mechanical modeling and design expressions: The Critical Shear Crack Theory for shear design, *Structural Concrete*, vol. 20, Issue 4, p. 1464-1480 https://doi.org/10.1002/suco.201900193

[15] Muttoni, A., Ruiz, M.F., and Sagaseta, J. (2015) Shear strength of concrete members without transverse reinforcement: A mechanical approach to consistently account for size and strain effects, *Engineering structures*, vol. 99, p. 360-372. https://www.sciencedirect.com/science/article/abs/pii/S0141029615003247

[16] Sarkhosh, R. *et al.* (2010) *Shear Capacity of Concrete Beams without Shear Reinforcement under Sustained Loads*. Literature survey. Delft University of Technology, Delft.

[17] Sørensen, S.I. (2013) *Betongkonstruksjoner - Beregning og dimensjonering etter Eurocode 2* Fagbokforlaget, Bergen.

[18] Turøy, L., Øzbal, A. and Aaserød, A. (2018) *Calculation methods for shear in NS-EN 1992-1-1:2004 and the new Eurocode draft, EC2:2017*. Master thesis. NTNU.

Appendix

A: Shear Transferring Mechanisms

Shear transferring mechanisms are the different mechanisms or actions that contribute to the shear carrying capacity after flexural cracks have started to develop in the concrete. The mechanisms are traditionally divided into two categories: beam shear-transfer actions and arching action. The beam shear-transfer actions include residual tensile strength in the concrete, cantilever action, dowel action caused by the longitudinal reinforcement, and interface shear transfer caused by aggregate interlock. The shear resistance in a concrete beam can almost always be described as a combination of the beam shear-transfer actions and the arching action [4]. Several suggestions have also been made of methods to calculate the magnitude of the contribution from each shear transfer mechanism to the final shear capacity [18] [2].

Beam Shear-Transfer Actions

Cantilever Action

When subjected to shear and bending, slender concrete members will develop flexural cracking long before the maximum capacity is reached. When the loading is continued and the depth of the cracks increases, the flexural cracks start to form a teeth-like pattern. Each 'tooth' can be seen as a concrete cantilever, where the longitudinal reinforcement contributes with a tensile force near the end [4].

The tensile forces in the cantilevers will be uneven, as the acting bending moment on the beam will vary along the direction of the longitudinal reinforcement. Assuming that the cracks do not transfer forces, the equilibrium has to be met by an inclined compression chord and an inclined tension tie internally in each cantilever[4]. The shear force will be carried by the inclination of the compression chord [2] [3]. Once the tension tie reaches the tensile strength of the concrete, the flexural crack will start propagating in a quasi-horizontal direction. The quasi-horizontal propagation will reduce the shear transfer capacity of the cantilever action [4]. A strut-and-tie model of the cantilever action is illustrated in Figure A.1a.

Aggregate Interlock

A fracture in concrete will never have a completely smooth or plane crack face. The aggregate particles along the crack face, combined with the uneven shape of the fracture itself, will give cause to frictional forces when the two sides attempts to slide against each other. This gives the crack shear carrying properties, as shear forces are being transferred from one side of the crack to the other [18] [16] [15].

Dowel Action

Dowel action is the effect from the longitudinal reinforcement, as each interface of a shear crack attempts to slide in separate transverse directions [18] [3]. The reinforcement will show some capacity to resist the transverse movement, and consequently transfer shear forces from one side of the crack to the other [16]. Dowelling action can give delamination fractures, as seen in Figure 2c.

Residual Tensile Strength

When cracks develop in a concrete member, the residual tensile strength of the concrete will help carry tensile stresses across the crack. As the cracks starts to progress, micro cracks will appear in the fracture process zone around the crack tip [3]. The micro cracks will then continue

to expand and merge together, eventually turning into macro cracks. The tensile stress in the concrete will decrease as the deformation increases, but the cracks will still have some shear transferring capacity until the crack width reaches 0.2 mm. After this point, the residual tensile stress is no longer considered to have any effect. The residual tensile strength contribution will be mainly governing in the quazi-horizontal part of the critical shear crack [4] [3].

Arching Action

The beam shear-transfer mechanisms consider the lever arm between the compression and tension chords as constant. Thus will the force in the longitudinal reinforcement vary with the bending moment of the beam [15]. When assuming the force in the longitudinal reinforcement is constant and sustain the same strain over the entire length of the beam, the shear load can be carried directly by an inclined compressive strut. This is referred to as the arching effect [18] [4]. In reality, a combination of the beam shear-transfer action and the arching action can happen at the same time [2].

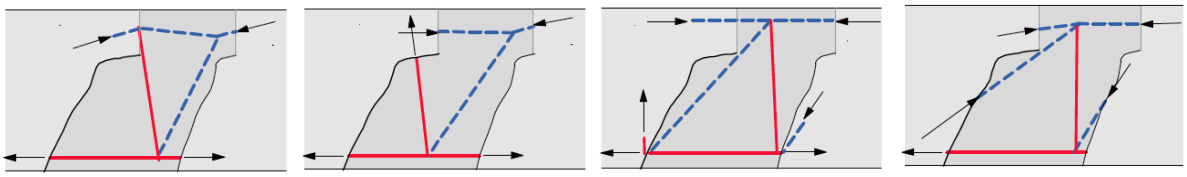

(a) Cantilever action **(b)** Aggregate interlock **(c)** Dowelling action **(d)** Residual tensile strength

Figure A.1: Strut-and tie model of the beam shear-transfer mechanisms (tensile forces in red and compressive forces in blue) [4]

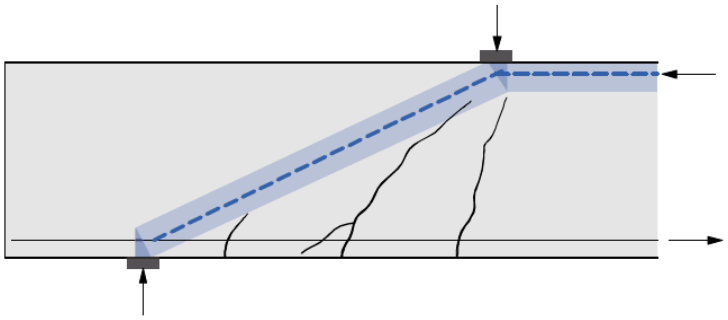

Figure A.2: Arching action in a beam, compressive arch illustrated in blue [4].

B: Calculations

f_c_cube [MPa]	f_c [MPa]
68,2	55,9
54,8	44,9
55,7	45,7
61,7	50,6
55,2	45,3
55,7	45,7
58,2	47,7
59,0	48,4
62,8	51,5

Figure B.1: Calculating the cylinder strength.

Shear capacity Eurocode 2

h [mm]	400
b [mm]	250
Ø [mm]	32
Ø' [mm] (co	25
As [mm^2]	2413
As' [mm^2]	982
Ac [mm^2]	100000
f_y [MPa]	550
d [mm]	344
Crdc	0,18
ro	0,02
k	1,76
k1	0,15
c_nom [mm	40

	sigma_cp [MPa]	Shear capacity EC2 [kN]
B1	0,00	131
B2	0,00	122
B3	0,00	123
B4	5,05	192
B5	5,01	187
B6	4,95	187
B7	8,02	228
B8	7,92	227
B9	7,90	230

Figure B.2: Shear capacity calculations based on Eurocode 2.

Shear capacity DNVGL ST-C502

W_c [mm^3]	6666666,7
I_c [mm^4]	1,333E+09
S_c [mm^3]	5000000
z_1	267
k_A [Mpa]	100
d_1 [mm]	1000
k_v (Between 1.0 and 1.4)	1,156
V_f [N]	250000
M_f [Nmm]	250000000

	Nf / Ac [MPa]	M_0 [Nmm]	f_t [MPa]	f_tn [MPa]	V_c0 [N]	V_c [kN]
B1	0,00	0,00E+00	3,59	2,47	1,47E+05	147
B2	0,00	0,00E+00	3,22	2,28	1,36E+05	136
B3	0,00	0,00E+00	3,24	2,29	1,37E+05	137
B4	5,05	3,37E+07	3,41	2,38	1,42E+05	169
B5	5,01	3,34E+07	3,23	2,28	1,36E+05	163
B6	4,95	3,30E+07	3,24	2,29	1,37E+05	163
B7	8,02	5,35E+07	3,32	2,33	1,39E+05	182
B8	7,92	5,28E+07	3,34	2,34	1,40E+05	182
B9	7,90	5,27E+07	3,44	2,40	1,43E+05	185

Figure B.3: Shear capacity calculations based on DNVGL-ST-C502.

Displacement

			Cracked stage (II)					Total deflection
	f_c [MPa]	Ecm [MPa]	n	alpha	(EI)2 [N mm^2]	Failure load V [kN]	delta_2 [mm]	Delta [mm]
B1	55,9	36872	5,70	0,43	2,94E+13	136	3,6	5,4
B2	44,9	34530	6,08	0,44	2,88E+13	124	3,4	5,1
B3	45,7	34700	6,05	0,44	2,88E+13	113	3,1	4,7
B4	50,6	35781	5,87	0,43	2,91E+13	184	4,9	7,5
B5	45,3	34606	6,07	0,44	2,88E+13	156	4,2	6,4
B6	45,7	34700	6,05	0,44	2,88E+13	169	4,6	7,0
B7	47,7	35160	5,97	0,44	2,90E+13	201	5,4	8,2
B8	48,4	35304	5,95	0,43	2,90E+13	196	5,3	8,0
B9	51,5	35971	5,84	0,43	2,92E+13	195	5,2	7,9

Es [Mpa]	210000
ro	0,03
a [mm]	1000
L [mm]	2750

Uncracked stage(I)

	alpha*d_1 [mm]	Ic_1 [mm^4]	Is_1 [mm^4]	(EI)1 [N mm^2]	delta_1 [mm]
B1	217	1,36E+09	3,87E+07	5,84E+13	1,8
B2	218	1,37E+09	3,80E+07	5,52E+13	1,7
B3	218	1,37E+09	3,81E+07	5,54E+13	1,6
B4	218	1,37E+09	3,84E+07	5,69E+13	2,5
B5	218	1,37E+09	3,81E+07	5,53E+13	2,2
B6	218	1,37E+09	3,81E+07	5,54E+13	2,4
B7	218	1,37E+09	3,82E+07	5,61E+13	2,8
B8	218	1,37E+09	3,83E+07	5,63E+13	2,7
B9	218	1,36E+09	3,84E+07	5,72E+13	2,7

Figure B.4: Calculated displacement.

Cracking Moment

	f_ctm [MPa]	Mcr_without_N [Nmm]	M_N [Nmm]	Total_Mcr [kNm]
B1	4,39	3,81E+07	0,00E+00	38
B2	3,79	3,34E+07	0,00E+00	33
B3	3,83	3,37E+07	0,00E+00	34
B4	4,10	3,58E+07	3,37E+07	70
B5	3,81	3,35E+07	3,34E+07	67
B6	3,83	3,37E+07	3,30E+07	67
B7	3,95	3,46E+07	5,35E+07	88
B8	3,98	3,49E+07	5,28E+07	88
B9	4,15	3,62E+07	5,27E+07	89

Figure B.5: Calculated flexural cracking moment.

Reinforcement stress at 0.5*critical shear load

alpha	Moment [Nmm]	(EI)_2[N mm^2]	sigma_s (MPa)
0,43	6,78E+07	2,94E+13	95
0,44	6,19E+07	2,88E+13	87
0,44	5,67E+07	2,88E+13	80
0,43	9,22E+07	2,91E+13	130
0,44	7,81E+07	2,88E+13	110
0,44	8,47E+07	2,88E+13	119
0,44	1,01E+08	2,90E+13	142
0,43	9,81E+07	2,90E+13	138
0,43	9,76E+07	2,92E+13	137

Figure B.6: Calculations of the reinforcement stress at 50% of the failure load.

EC2 and DNVGL-ST-C502 shear capacity with safety factors

		N [kN]	sigma_cp [Mpa]	V EC2 with SF	Nf/Ac [MPa]	M_0 [Nmm]	V_co [N]	V DNVGL with SF[kN]
f_c_average [MPa]	48,4	0	0,0	79	0,0	0,00E+00	8,70E+04	87
f_ck_average [MPa]	40,4	50	0,5	85	0,5	3,33E+06	8,70E+04	90
f_cd_average [MPa]	22,9	100	1,0	92	1,0	6,67E+06	8,70E+04	92
f_tk [MPa]	3,05	150	1,5	98	1,5	1,00E+07	8,70E+04	95
f_td	1,46	200	2,0	104	2,0	1,33E+07	8,70E+04	98
f_tn [MPa]	2,19	250	2,5	111	2,5	1,67E+07	8,70E+04	100
		300	3,0	117	3,0	2,00E+07	8,70E+04	103
		350	3,5	124	3,5	2,33E+07	8,70E+04	106
		400	4,0	130	4,0	2,67E+07	8,70E+04	108
		450	4,5	137	4,5	3,00E+07	8,70E+04	111
		500	4,6	138	5,0	3,33E+07	8,70E+04	114
		550	4,6	138	5,5	3,67E+07	8,70E+04	116
		600	4,6	138	6,0	4,00E+07	8,70E+04	119
		650	4,6	138	6,5	4,33E+07	8,70E+04	122
		700	4,6	138	7,0	4,67E+07	8,70E+04	124
		750	4,6	138	7,5	5,00E+07	8,70E+04	127
		800	4,6	138	8,0	5,33E+07	8,70E+04	130

Figure B.7: Calculations of the shear capacities from Eurocode 2 and DNVGL-ST-C502 with all safety factors.

C: Load - Displacement Diagrams

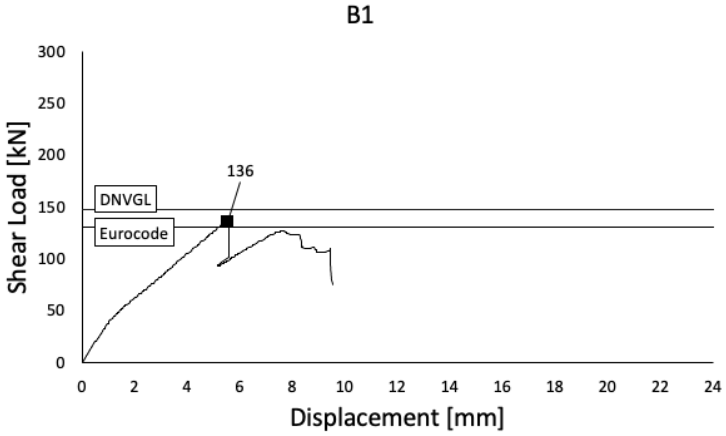

Figure C.1: Load-Displacement diagram for B1.

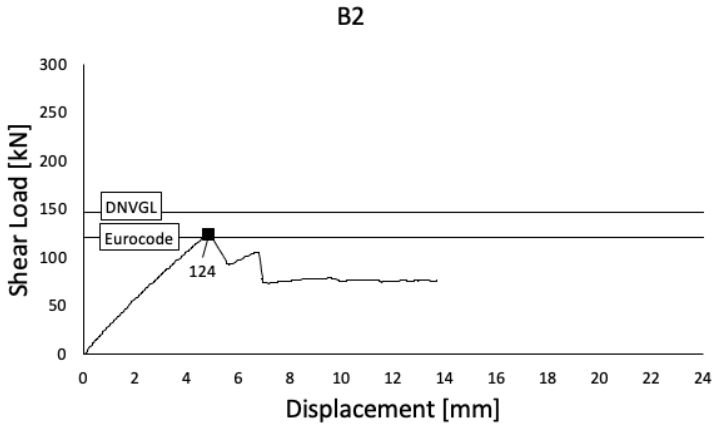

Figure C.2: Load-Displacement diagram for B2.

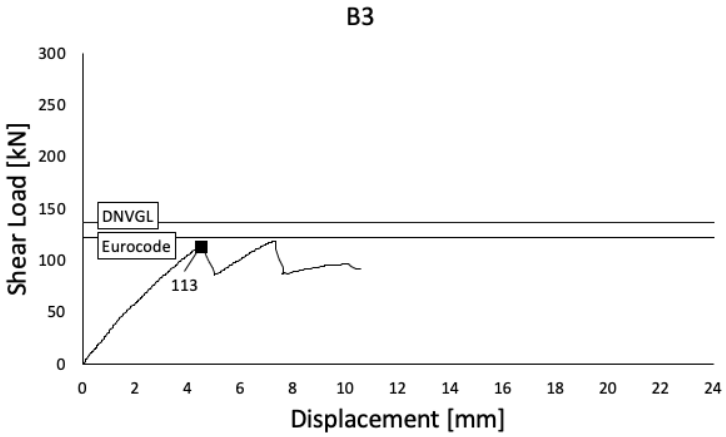

Figure C.3: Load-Displacement diagram for B3.

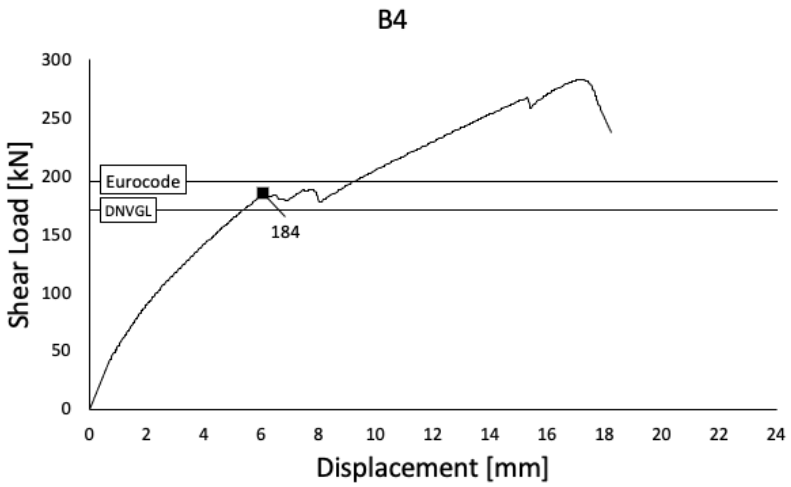

Figure C.4: Load-Displacement diagram for B4.

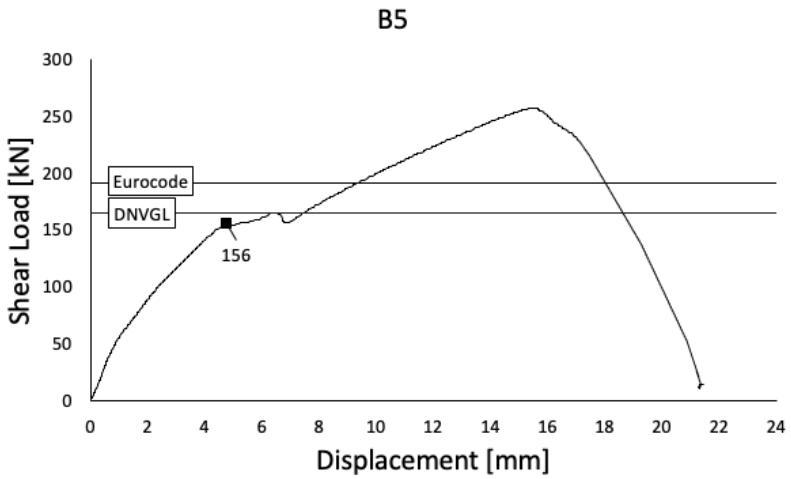

Figure C.5: Load-Displacement diagram for B5.

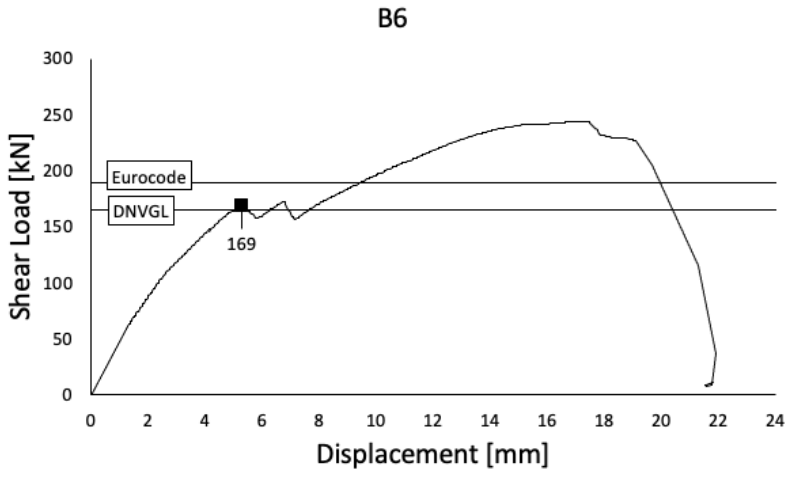

Figure C.6: Load-Displacement diagram for B6.

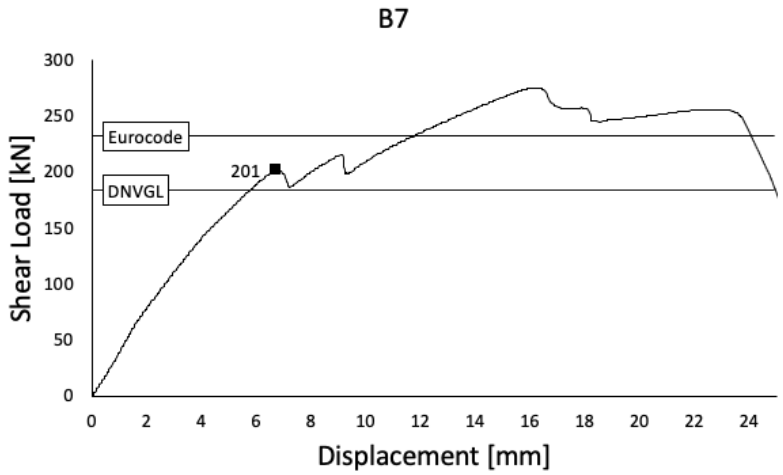

Figure C.7: Load-Displacement diagram for B7.

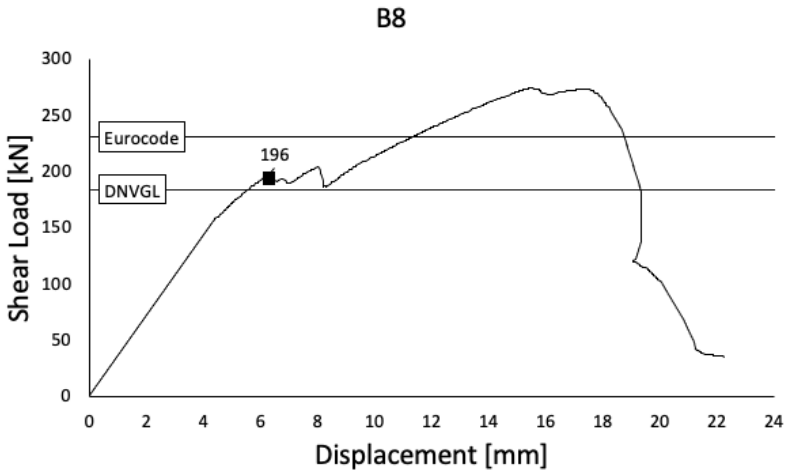

Figure C.8: Load-Displacement diagram for B8.

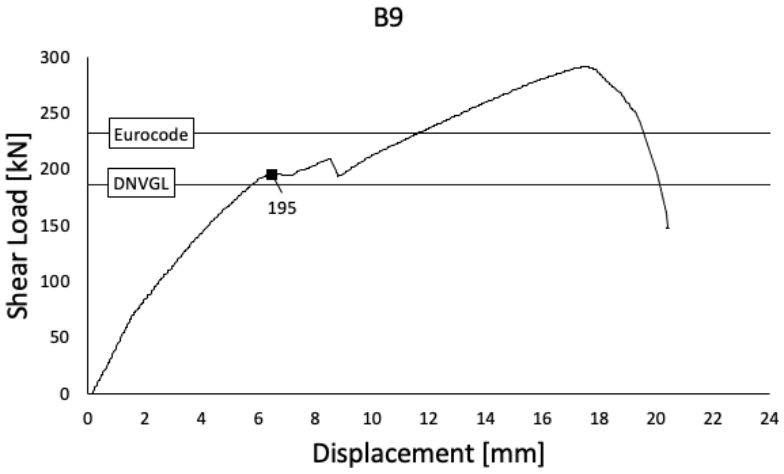

Figure C.9: Load-Displacement diagram for B9.

D: Crack Development Pictures

Beam B1 without Axial Load

Figure D.1: Shear crack in B1 in connection with the first peak in the load - displacement graph.

Figure D.2: Shear crack in B1 after the second peak in the load - displacement graph.

Beam B2 without Axial Load

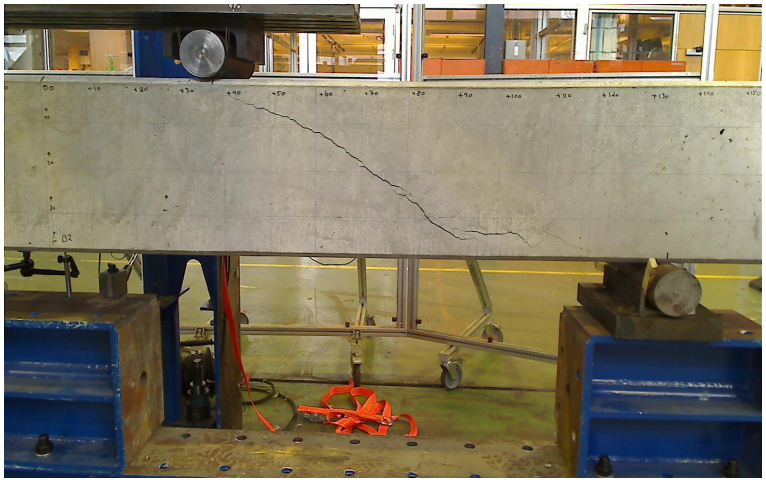

Figure D.3: Shear crack in B2 in connection with the first peak in the load - displacement graph.

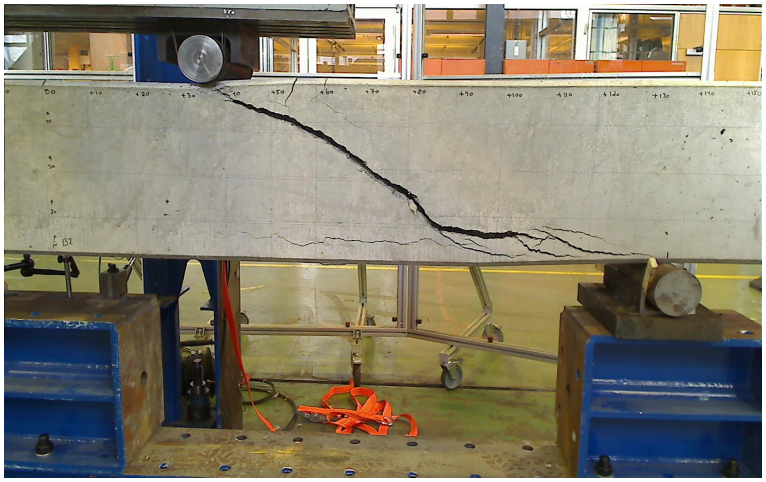

Figure D.4: Shear crack in B2 after the second peak in the load - displacement graph.

Beam B3 without Axial Load

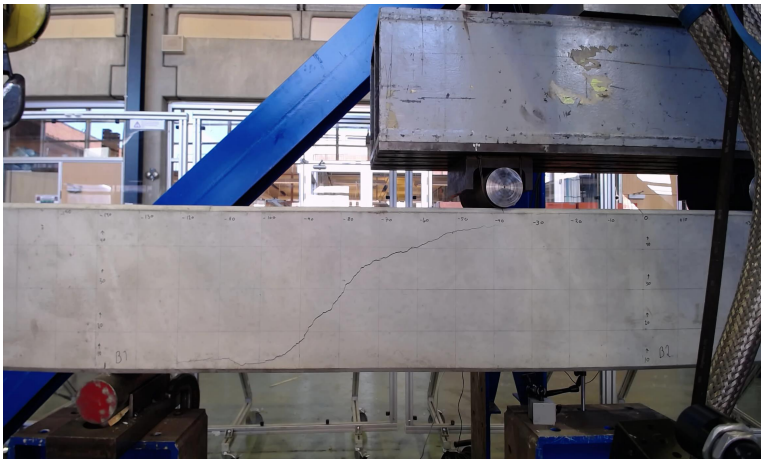

Figure D.5: Shear crack in B3 in connection with the first peak in the load - displacement graph.

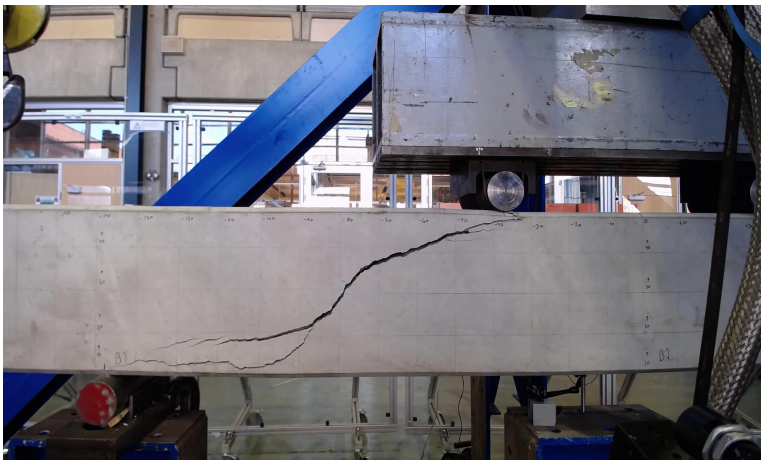

Figure D.6: Shear crack in B3 after the second peak in the load - displacement graph.

Beam B4 with an Axial Load of 500 kN

Figure D.7: Shear crack in B4 in connection with the first peak in the load - displacement graph.

Figure D.8: B4 before the second peak.

Figure D.9: Shear crack in B4 after the second peak in the load - displacement graph.

Beam B5 with an Axial Load of 500 kN

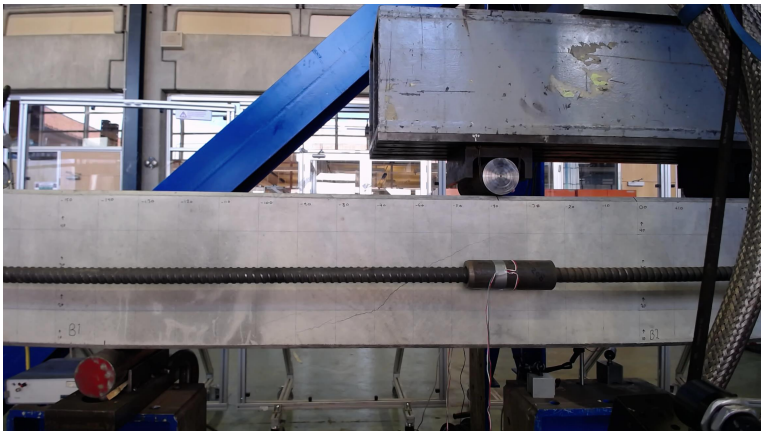

Figure D.10: Shear crack in B5 in connection with the first peak in the load - displacement graph.

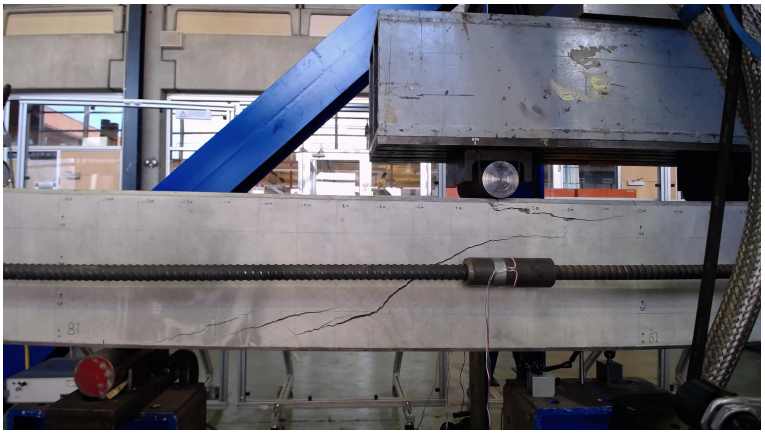

Figure D.11: B5 before the second peak.

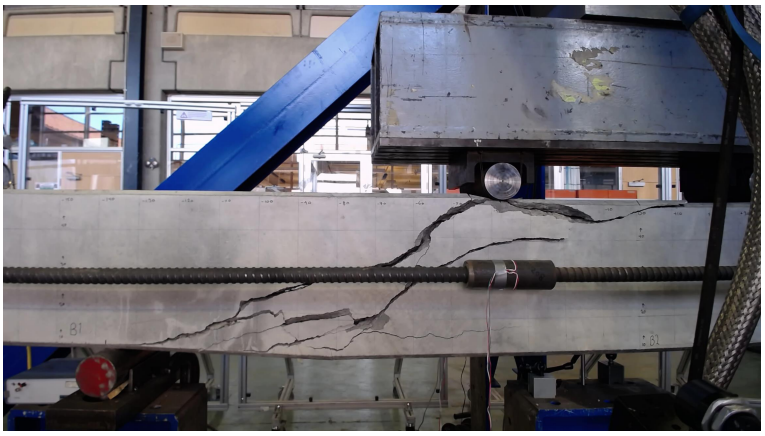

Figure D.12: Shear crack in B5 after the second peak in the load - displacement graph.

Beam B6 with an Axial Load of 500 kN

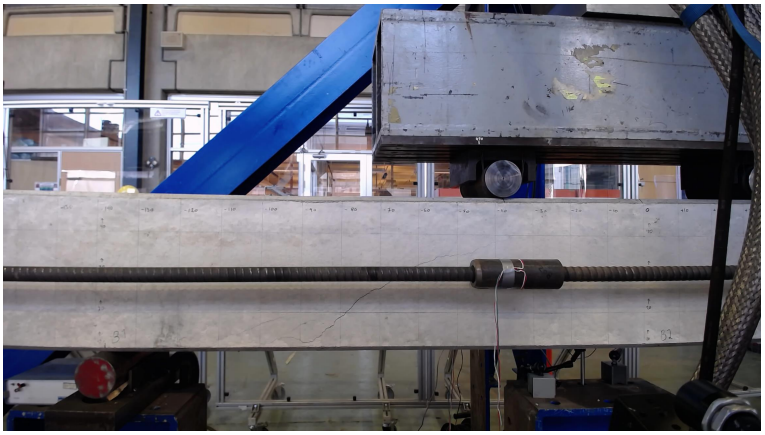

Figure D.13: Shear crack in B6 in connection with the first peak in the load - displacement graph.

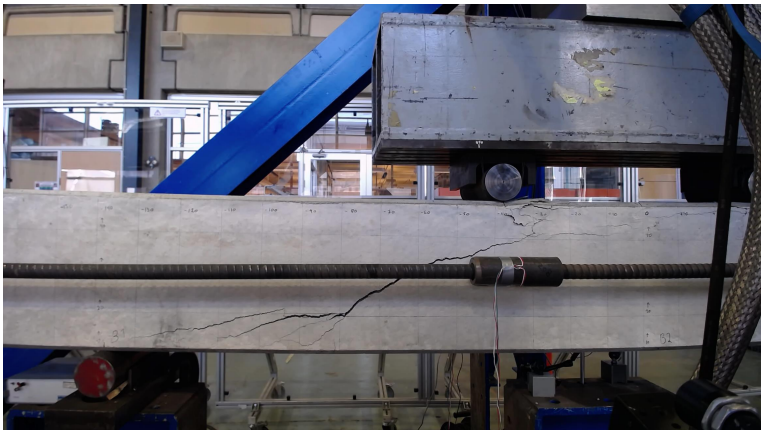

Figure D.14: B6 before the second peak.

Figure D.15: Shear crack in B6 after the second peak in the load - displacement graph.

Beam B7 with an Axial Load of 800 kN

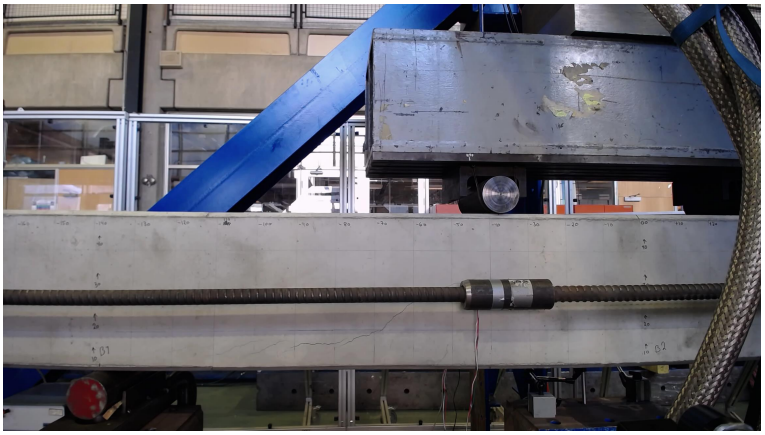

Figure D.16: Shear crack in B7 in connection with the first peak in the load - displacement graph.

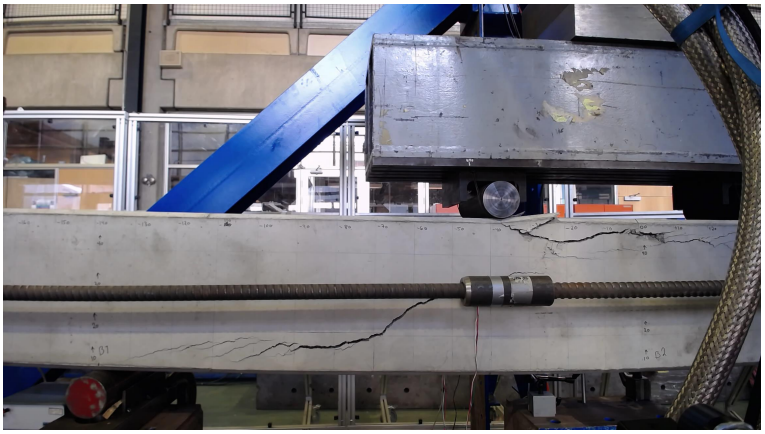

Figure D.17: B7 before the second peak.

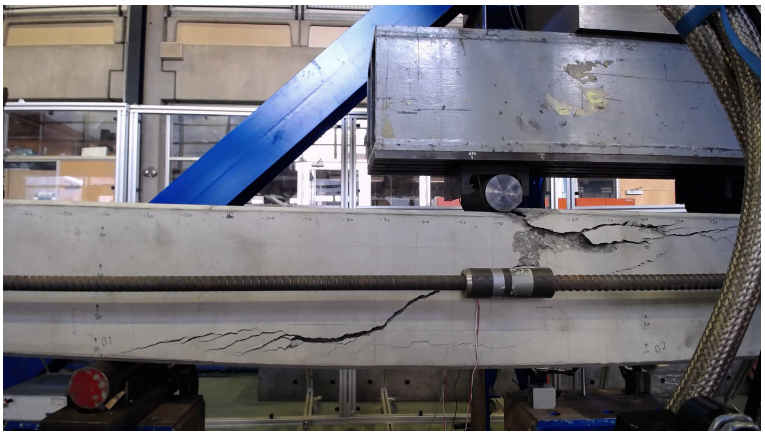

Figure D.18: Shear crack in B7 after the second peak in the load - displacement graph.

Beam B8 with an Axial Load of 800 kN

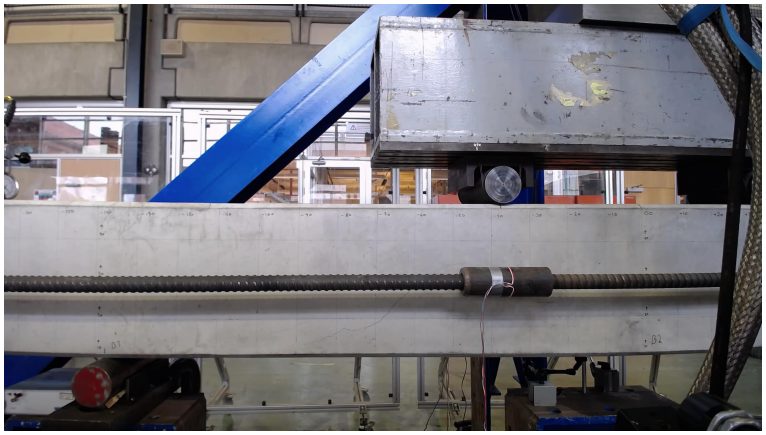

Figure D.19: Shear crack in B8 in connection with the first peak in the load - displacement graph.

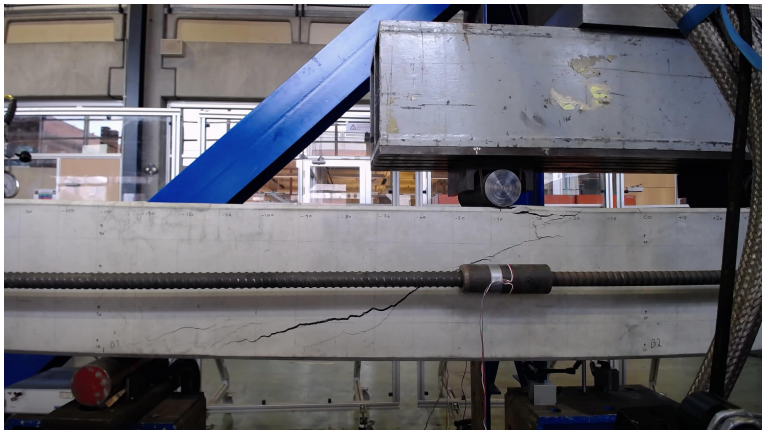

Figure D.20: B8 before the second peak.

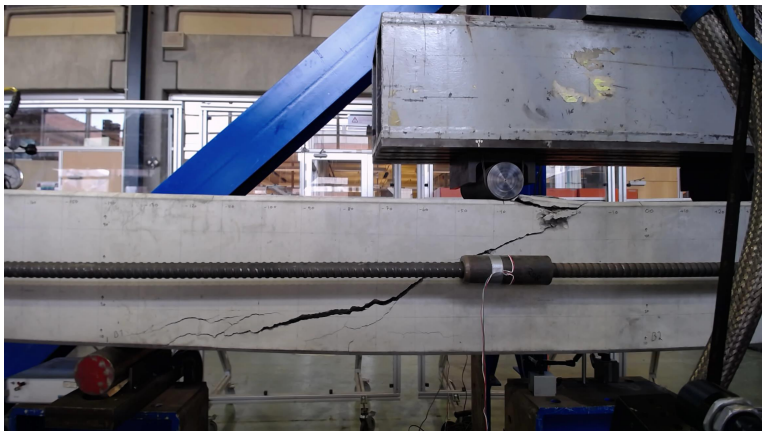

Figure D.21: Shear crack in B8 after the second peak in the load - displacement graph.

Beam B9 with an Axial Load of 800 kN

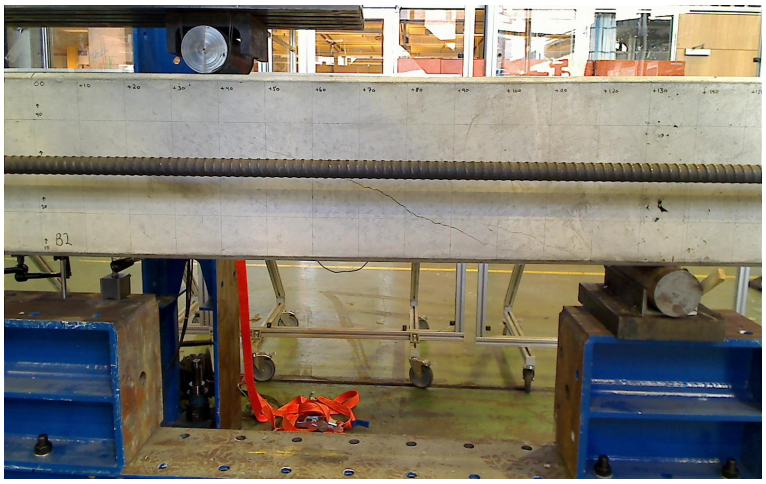

Figure D.22: Shear crack in B9 in connection with the first peak in the load - displacement graph.

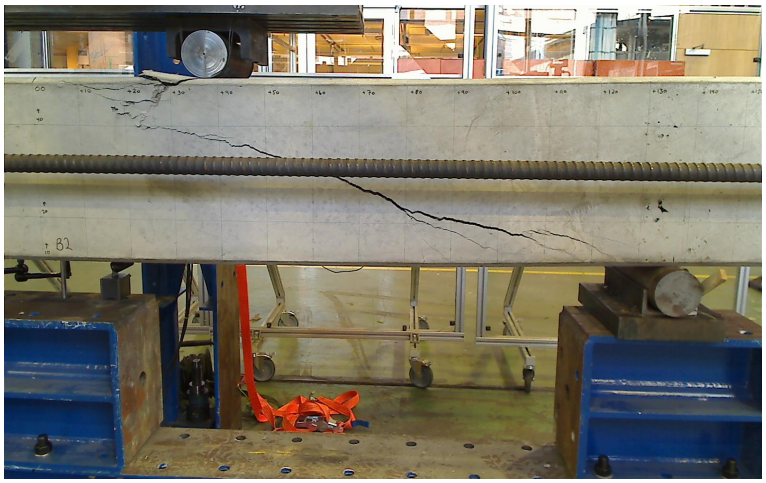

Figure D.23: B9 before the second peak.

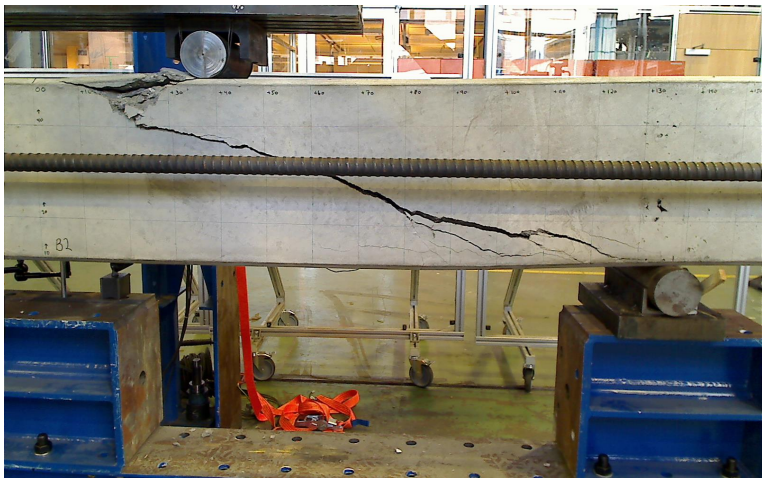

Figure D.24: Shear crack in B9 after the second peak in the load - displacement graph.

E: Compressive Cube Strength Report

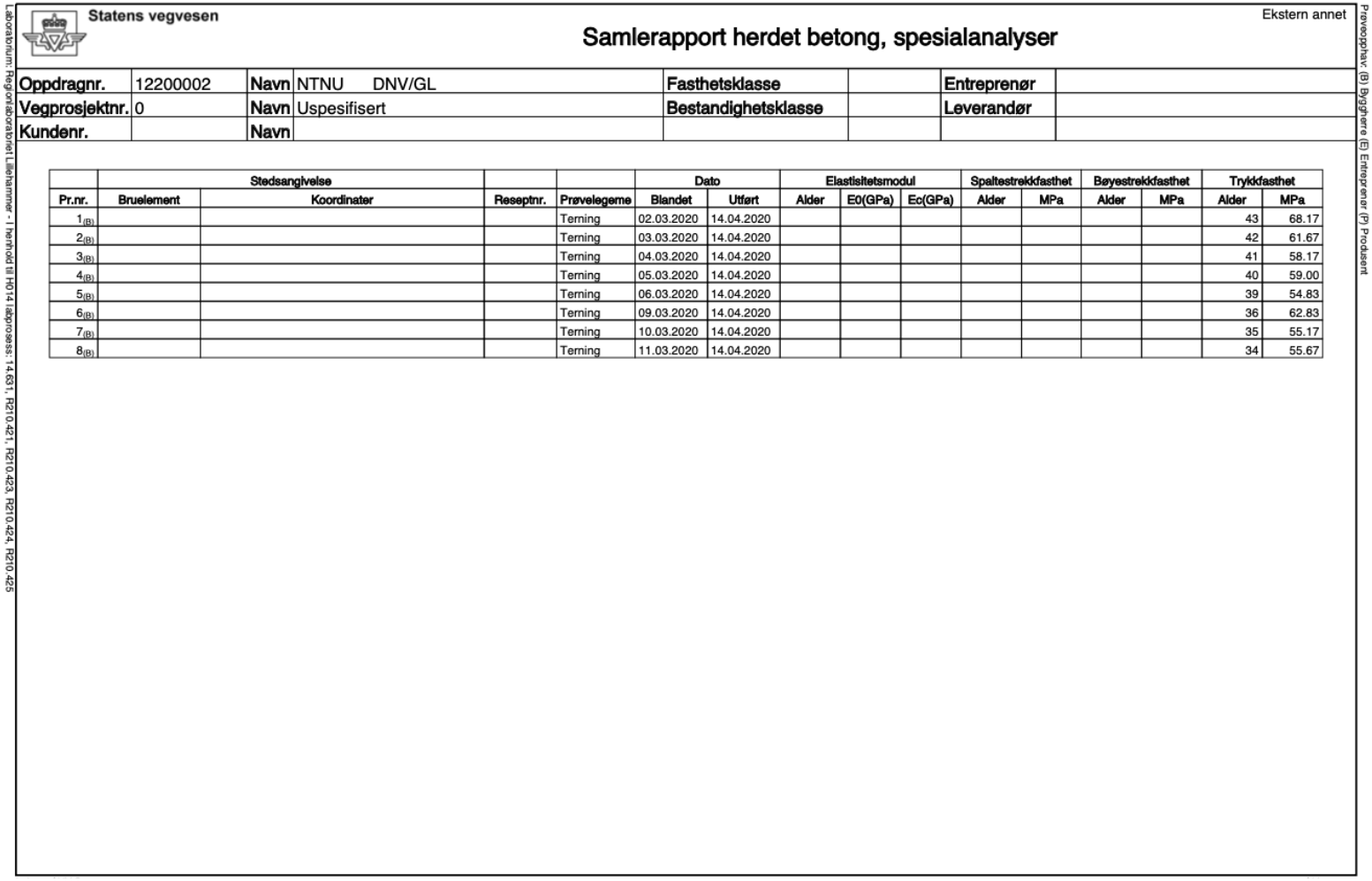

Statens vegvesen

Ekstern annet

Samlerapport herdet betong, spesialanalyser

Oppdragnr.	12200002	**Navn**	NTNU DNV/GL	**Fasthetsklasse**		**Entreprenør**	
Vegprosjektnr.	0	**Navn**	Uspesifisert	**Bestandighetsklasse**		**Leverandør**	
Kundenr.		**Navn**					

	Stedsangivelse				Dato		Elastisitetsmodul			Spaltestrekkfasthet		Bøyestrekkfasthet		Trykkfasthet	
Pr.nr.	**Bruelement**	**Koordinater**	**Reseptnr.**	**Prøvelegeme**	**Blandet**	**Utført**	**Alder**	**E0(GPa)**	**Ec(GPa)**	**Alder**	**MPa**	**Alder**	**MPa**	**Alder**	**MPa**
1(B)				Terning	02.03.2020	14.04.2020								43	68.17
2(B)				Terning	03.03.2020	14.04.2020								42	61.67
3(B)				Terning	04.03.2020	14.04.2020								41	58.17
4(B)				Terning	05.03.2020	14.04.2020								40	59.00
5(B)				Terning	06.03.2020	14.04.2020								39	54.83
6(B)				Terning	09.03.2020	14.04.2020								36	62.83
7(B)				Terning	10.03.2020	14.04.2020								35	55.17
8(B)				Terning	11.03.2020	14.04.2020								34	55.67

Laboratorium: Regionlaboratoriet Lillehammer - I henhold til H014 laboprosess: 14.631, R210.421, R210.423, R210.424, R210.425

Prøvested/hav: (B) Byggherre (E) Entreprenør (P) Produsent

Figure E.1: Load-displacement diagrams for beams B1-B9, with calculated capacities found in Eurocode 2 and DNVGL-ST-C502.

NTNU
Norwegian University of
Science and Technology

DNV·GL